

Numerical Optimal Control of Hybrid Electric Trucks: Exhaust Temperature, NO_x Emission and Fuel Consumption

Fredrik Andersson and Hampus Andersson

Master of Science Thesis in Electrical Engineering
**Numerical Optimal Control of Hybrid Electric Trucks: Exhaust Temperature,
NO_x Emission and Fuel Consumption**

Fredrik Andersson and Hampus Andersson

LiTH-ISY-EX--18/5137--SE

Supervisor: **Olov Holmer**
ISY, Linköping University
Viktor Leek
ISY, Linköping University

Examiner: **Lars Eriksson**
ISY, Linköping University

*Division of Automatic Control
Department of Electrical Engineering
Linköping University
SE-581 83 Linköping, Sweden*

Copyright © 2018 Fredrik Andersson and Hampus Andersson

Abstract

The controls for a parallel hybrid electric truck are optimized using numerical optimal control. Trade-offs between catalyst light-off times, NO_x emission and fuel consumption have been investigated for cold starts at two operating points, as well as temperature differences between conventional and hybrid powertrains during WHTC (World Harmonized Transient Cycle). A model describing the temperature dynamics of the aftertreatment system is implemented as well as temperature-based de NO_x performance for both Cu-Zeolite and Fe-Zeolite catalysts. Control is performed in a piecewise linear fashion, resulting in a total of 23 states including control signals. It is shown that high temperatures can be a larger threat to catalyst performance when running the WHTC than low temperatures, for both conventional and hybrid powertrains. Furthermore, decreasing the light-off time of the catalyst does not always lead to decreased NO_x emission, instead there is a trade-off between light-off time and NO_x emission. It is found that there are controls that will realize decreased NO_x emission for a hybrid truck during cold starts at the expense of increased fuel consumption.

Acknowledgments

The last six months have been very evolving for us as future engineers as this is our largest project yet. First and foremost, we would like to express our sincere gratitude to Olov Holmer and Viktor Leek for their availability for questions and for the worthwhile discussions every Friday meeting. Your genuine interest and knowledge in the field is always inspiring!

Thank you Lars Eriksson for taking the time to discuss with us whatever trouble that is on our minds, even though we know you are a busy man. We hope you've enjoyed all the weekly plots and graphs we sent you.

The Department of Vehicular Systems has offered us a welcoming atmosphere with lots of interesting and nerdy (but entertaining, for sure) conversations in the coffee-room. The free coffee is surely a contributing factor in the writing of this report. On the topic of coffee, thank you Sebastian Kramarz for your company during many traditional Swedish 'fika' and walks around campus!

We would like to extend our gratitude to Scania for providing this thesis opportunity and Verena Klass in particular for her feedback. This project was supported by the *Swedish Governmental Agency for Innovation Systems* under the program *Strategic Vehicle Research and Innovation*, grant FROST (2016-05380).

Linköping, June 2018
Fredrik and Hampus

Contents

Notation	ix
1 Introduction	1
1.1 Objective	1
1.2 Related research	2
1.3 Delimitations	4
2 Theory and background	5
2.1 Catalysis	5
2.2 Emissions and aftertreatment	7
2.2.1 Diesel oxidation catalyst	9
2.2.2 Diesel particulate filter	9
2.2.3 Selective catalytic reduction	10
2.2.4 Ammonia slip catalyst	12
2.3 Emission standards	14
3 Optimization environment	17
3.1 Development procedure	17
3.2 Lookup tables	18
3.3 Denormalization of WHTC	21
3.4 Solver initial guess	21
3.5 Model description	21
3.5.1 Electric motor	22
3.5.2 Battery	24
3.5.3 Diesel engine	25
3.5.4 Aftertreatment system	28
3.6 Optimization limitations	32
4 Results	33
4.1 WHTC temperature and deNO _x comparison	33
4.2 Optimal control for cold start	39
4.2.1 High load operating point	39
4.2.2 Low load operating point	48

4.3	Steady state NOx versus light-off time tradeoff	57
4.4	Steady state fuel versus NOx trade-off	58
5	Discussion	63
6	Conclusions	65
6.1	Future work	66
A	WHTC denormalization	69
A.1	Engine speed profile	69
A.2	Torque profile	70
B	Solver initial guess - Alternative approaches	73
B.1	Constant torque-split with feedback	73
B.2	Equivalent Consumption Minimization Strategy	74
	Bibliography	77
	Index	81

Notation

ABBREVIATIONS

Abbreviation	Meaning
ASC	Ammonia slip catalyst
BMS	Battery monitoring system
DEF	Diesel exhaust fluid
DOC	Diesel oxidation catalyst
DP	Dynamic programming
DPF	Diesel particulate filter
EATS	Exhaust aftertreatment system
ECMS	Equivalent consumption minimization strategy
EM	Electric motor
EPA	US Environmental Protection Agency
FTP	Federal Test Procedure
HD	Heavy duty
HEV	Hybrid electric vehicle
ICE	Internal combustion engine
NHTSA	National Highway Traffic Safety Administration
NLP	Non-linear program
NOX	Nitrous oxide (NO or NO_2)
OCP	Optimal control problem
PM	Particulate matter
PMP	Pontryagin's Minimum Principle
SCR	Selective catalytic reduction
SOC	State of charge
WHSC	World harmonized stationary cycle
WHTC	World harmonized transient cycle

1

Introduction

Hybrid electric vehicles (HEVs) have seen a surge in popularity due to the ever increasing demands placed on emissions and efficiency. This has opened up a new field of issues relating to the additional degree of freedom provided by the dual energy sources. The answer to the question of when to use the electric motor (EM) and when to use the internal combustion engine (ICE) can vary depending on what end result is desired. In the case of minimizing fuel consumption, techniques such as the Equivalent Consumption Minimization Strategy (ECMS) are well established.

While the solution provided by ECMS is near-optimal [7], it does not account for the natural cooling of the exhaust system that occurs during prolonged electric propulsion, potentially leading to increased particulate emissions due to the catalyst falling below its operating temperature. Re-heating of the exhaust system requires additional energy in some form, usually provided by the combustion of additional fuel. This detracts somewhat from the apparent benefits offered by hybridization. In order to maximize the use of the hybrids potential as an environmentally friendly technology, it is of interest to ascertain the optimal balance between fuel economy and heat generation required to maintain functionality of the aftertreatment system.

1.1 Objective

The main focus of this thesis is to investigate the optimal control of a parallel electric hybrid diesel truck with respect to maintaining low out-of-pipe emissions while minimizing fuel consumption throughout a chosen driving cycle. The efficiency of the deNO_x system is directly correlated to the temperature of the catalyst.

Power distribution for HEVs can be improved by taking into account engine and catalyst temperatures in addition to the state of charge (SOC) and engine speed used by established methods such as ECMS and dynamic programming (DP). The increase in dimension caused by these additional states is severely impairing to such methods, which is why a new optimization environment will be devised using numerical optimal control methodology. This environment should allow for analysis of the trade-off between, for instance, fuel mass flow and NO_x emission. The performance and applicability of the described method can then be compared to those of DP and ECMS where possible. Questions answered in the process of such an analysis, and the outline of a workflow, are:

- Which temperatures occur in the diesel engine and exhaust system during WHTC and steady-state conditions, and are there operating conditions where they fall below the values required by the exhaust system?
- Comparing a conventional powertrain with a hybrid powertrain, how does the exhaust system temperature change under the same driving conditions, and how does this affect NO_x reduction?
- Comparing a conventional powertrain with a hybrid powertrain, what are the optimal cold-start strategies with respect to fuel consumption and NO_x ? What are their differences and similarities?
- Does combustion of fuel for the purpose of heating the catalyst improve deNO_x performance, and if so, what is the fuel cost per NO_x reduction?
- Is numerical optimal control a suitable method for this type of problem?

1.2 Related research

Dynamic programming (DP) is a method described by Richard Bellman as a way of treating multi-stage decision processes [4], which provides the global optimum by minimizing a cost function. It has been applied extensively when calculating the power distribution of HEVs, where the decision being made is whether to use the ICE or the EM. DP suffers from the drawback that it requires some knowledge of the route *a priori* [27], which is not always available. Furthermore, significant computational effort is involved and its complexity grows exponentially with the number of states included, referred to as the *curse of dimensionality*. Due to these limitations DP is not considered viable as an online control strategy [13] but may rather (in the general case) serve as a benchmark comparison for other methods.

A comparison between DP and ECMS shows that the latter may provide a local or global optimum depending on the fulfillment of certain criteria, with little practical difference in results when compared to DP [7]. It could therefore potentially serve as a benchmark instead of DP. ECMS is based on Pontryagin's minimum principle (PMP), and associates power consumption from the battery with future

fuel consumption via a so called Hamiltonian which, when minimized, provides an optimal control trajectory with respect to fuel consumption [13]. Because the costate of the Hamiltonian relating to SOC can be assumed constant, its value can be computed at every instant with a feedback, allowing for online use.

Although it was stated in the introduction of this thesis that ECMS does not take into account the heat transfer of the engine and exhaust system, Serrao *et al.* [32] have shown how boundary conditions and cost function can be modified to include additional states such as temperature or emissions. However, the costates related to these added states vary with coupled dynamics and thus cannot be assumed constant. In the study, the initial values for these costates are searched for manually and the authors conclude that implementation of the strategy is difficult offline and impossible online for the case of engine and catalyst temperatures.

Kessels *et al.* [34] have evaluated the tradeoff between operational cost and NO_x emissions for a series hybrid truck. By using driveline- and aftertreatment models they estimated the monetary cost of consumed fuel and AdBlue and weighted it against emissions on hamiltonian form, using PMP. This allowed them to plot optimal trajectories through the ICE efficiency map for minimization of cost or emissions, as well as the combined solution. Simulation results using the Federal Test Procedure cycle showed that there was little room for influence with regard to cost due to the fixed power demand of the cycle and the constant cost of fuel, whereas the emissions could be controlled over a larger range. They also noticed how, when minimizing emissions, some constant power outtake from the ICE remained in regions where the cost effective optimization had turned it off, thus preventing the temperature from dropping. Furthermore, in these regions, the power outtake from the ICE was used to charge the battery.

Ma and Wang [28] have developed an integrated model based strategy for a parallel HEV which takes into account fuel consumption, NO_x emissions, ammonia slip and road grade. The case of ammonia slip is interesting because when targeting high NO_x conversion, more urea is injected into the exhaust gases. If the urea quantity is too large in proportion to NO_x , ammonia will exit with the tailpipe emissions without reacting. Effectively, reducing one pollutant can cause an increase of the other. The strategy presented, however, showed reduced fuel consumption, NO_x emissions and ammonia slip when compared to another unspecified energy management strategy, indicating that proper control can allow for such paradoxical phenomena to be circumnavigated.

Direct methods of numerical optimal control can be used to approximate a continuous problem with a finite nonlinear program for which solution methods exist. Two such methods are direct multiple shooting and direct collocation. Direct multiple shooting discretizes the time into finite segments for each of which an initial piece-wise constant control is guessed. The states are then integrated independently over each segment based on these controls and end-value constraints

help to sew together the segments. Direct collocation is a method in which the time is discretized into segments, each containing a chosen number of so-called collocation points. A polynomial is fitted so that its value and derivative coincide with those of the states in these points, but is free to deviate in between.

1.3 Delimitations

The scope of this thesis has been limited in order to ensure continuous progress. The delimitations are listed below, but may also be discussed further in relevant chapters.

- No complete vehicle model is investigated. Only the driveline and aftertreatment system is present.
- The investigated driveline is of a parallel hybrid configuration.
- The throttle is fully opened in all experiments.
- No urea injection or ammonia slip models are implemented.
- The direct collocation optimization method is used in all experiments.

2

Theory and background

In this chapter the theory of catalysis, aftertreatment and related components is presented in order to provide necessary background knowledge.

2.1 Catalysis

Catalysis is a phenomenon where an additional substance (called catalyst) is used to increase the rate of a chemical reaction without consuming the substance. In the automotive application, heterogeneous catalysts are commonly used. The heterogeneity comes from the catalyst being solid and the reactants being in gas phase. The catalyst substance is usually introduced as a washcoat on the surface of an inert porous structure on which the reactions take place [10].

For a reaction to occur, a certain activation energy has to be supplied to the reactants. This activation energy can be reduced significantly by a catalyst, which will adsorb the reactants. In their adsorbed state, only a small amount of additional energy is required for the reactants to undergo their desired reaction and desorb from the catalyst. A comparison between the normal and catalytic reaction processes is seen in Figure 2.1. It is the heat in the exhaust system that supplies the catalytic activation energy, which is why the temperature is of importance. The reaction rate k can be described by the Arrhenius Equation (2.1),

$$k = A \cdot e^{-\frac{E_a}{RT}} \quad (2.1)$$

where A is the reaction rate if there was no required activation energy, according to the kinetic molecular theory. This rate is then affected by the ratio between activation energy E_a and the kinetic energy RT , where R is the gas constant and

T is temperature. The dependence of the reaction rate on temperature is usually visualized by rewriting Equation (2.1) on the form of Equation (2.2), the plot of which can be seen in Figure 2.2.

$$\ln(k) = \ln(A) - \frac{E_a}{RT} \quad (2.2)$$

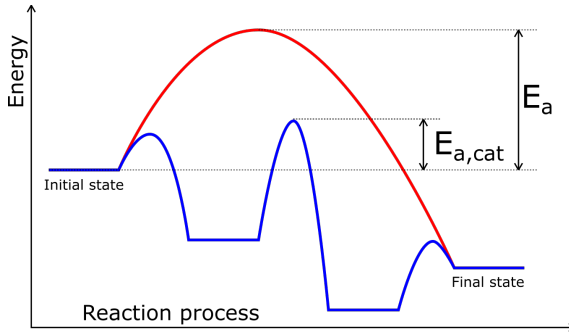


Figure 2.1: Comparison between regular and catalytic reaction in terms of energy required. Blue curve is the catalytic reaction which proceeds in three steps, adsorption, reaction and desorption. The red curve is the regular reaction which happens in one step, requiring more activation energy.

In automotive applications, a heterogeneous catalyst is used and bound in a wash-coat on a metal and ceramic structure designed for large surface area. There are a number of used compositions of catalyst used in automotive catalysts, all with their special properties. Vanadium-based, copper-Zeolite (Cu-Zeolite) or iron-Zeolite (Fe-Zeolite) is the most common catalyst in SCR catalysts for mobile diesel engines [23]. Cu-Zeolite enables better deNO_x performance at lower temperatures than Fe-Zeolite, but Fe-Zeolite outperform Cu-Zeolites at higher temperatures. Girard *et al.* has shown that a combination of Cu-Zeolite and Fe-Zeolite can give a good compromise between the benefits and drawbacks of the two [35].

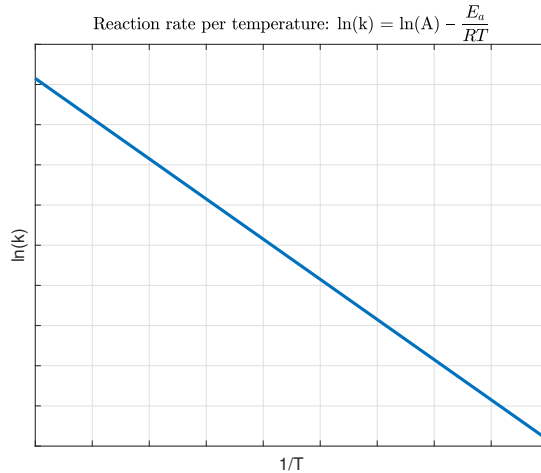


Figure 2.2: Relationship between reaction rate and temperature according to the Arrhenius equation, where the slope is E_a/R

2.2 Emissions and aftertreatment

Diesel is composed of hydrocarbons (HC), and the chemical formula is in the range of $C_{10-20}H_{8-42}$. When combusted, a number of substances that are harmful to health and environment are formed. [11]

Carbon monoxide (CO) is directly harmful to human health, with symptoms ranging from cardiovascular and neurobehavioral effects to unconsciousness and death depending on the level of exposure [15]. Nitric oxide (NO) and nitrogen dioxide (NO_2), collectively referred to as NO_x , are greenhouse gasses which also contribute to smog and acid rain which in turn contributes to acidification of the local environment [17]. Particulate matter (PM), has been linked to respiratory and cardiovascular diseases [41]. In order to mitigate these effects the exhaust gasses from the engine pass through an aftertreatment system in which various chemical reactions convert the harmful substances into less severe ones.

For a heavy duty diesel truck, such a system can contain a plethora of components. In the studied case, the aftertreatment system consists of components in the following order:

1. Diesel Oxidation Catalyst (DOC)
2. Diesel Particulate Filter (DPF)
3. Selective Catalytic Reduction (SCR) + AdBlue
4. Ammonia Slip Catalyst (ASC)

An illustration of this exhaust system can be seen in Figure 2.3 and the individual components are described in detail section-wise below.

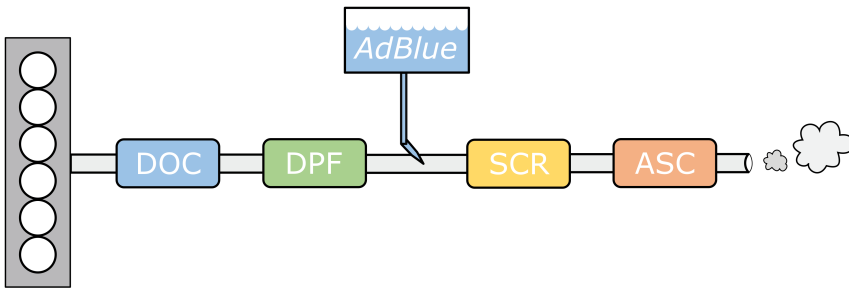


Figure 2.3: Schematic overview of the aftertreatment system for the heavy duty truck examined.

2.2.1 Diesel oxidation catalyst

The first step in the aftertreatment system is a diesel oxidation catalyst, whose function has been described extensively by Russel and Epling [33]. They describe that the traditional function of the DOC is to oxidize HC and CO which are formed by incomplete fuel combustion. These substances are adsorbed to the surface of the catalyst along with oxygen with which they react. HC and CO can both inhibit conversion of the other due to competitive adsorption onto the catalyst.

Nitrogen present in the air is also oxidized in the DOC, giving rise to NO and NO₂. A portion of NO (which constitutes approximately 90% of the NO_x) can be converted into NO₂ in the DOC according to Equation (2.3), which is beneficial to the function of downstream components.



Russel and Epling also note that controlling both NO_x and PM at the same time is difficult below certain temperatures; 200-300 °C for light-duty engines and 300-450 °C for heavy-duty engines.

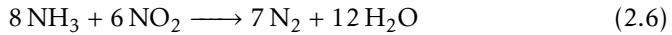
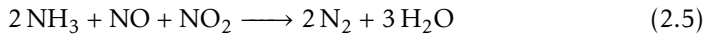
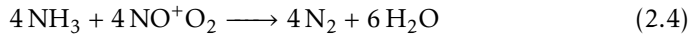
In a study of *Pt-Pd* catalysts, Balakotaiah *et al.* [18] showed results pertaining to light-off temperatures for different constituents in diesel exhaust. The temperatures differed based on the *Pt:Pd* ratio, but ranged between 180-230 °C for CO and 230-330 °C for various hydrocarbons, and for a standard mixture of CO and HC remained within the span 180-330 °C. The pure *Pd* catalyst showed the lowest light-off temperatures for most of the constituent substances, which is due to *Pd* having a lower light-off temperature for CO, thus reducing the inhibition of HC conversion.

2.2.2 Diesel particulate filter

The next step is a diesel particulate filter, whose main function is to trap particles present in the exhaust gases. Such a filter consists of multiple parallel channels into which the exhaust gases flow. Half of these channels are blocked at the inlet side and the other half is blocked on the outlet side, forcing the entering gasses to pass through the porous wall separating the channels, leaving its particles behind. PM will accumulate in the filter over time, leading to decreased efficiency. Techniques for counteracting these effects are referred to as 'regeneration', and usually depend on combustion or catalysis [33].

2.2.3 Selective catalytic reduction

This is where the benefits of the $\text{NO} \rightarrow \text{NO}_2$ conversion in the DOC are reaped. After leaving the DOC and DPF, ammonia (NH_3) is added to the exhaust gases before reaching another catalyst where they are subject to selective catalytic reduction. SCR reduces NO and NO_2 emissions by either of three reactions:



Where (2.4) is referred to as a standard SCR reaction, (2.5) is a fast SCR reaction, and (2.6) is a slow ditto. It is the fast reaction that is facilitated by the presence of NO_2 in addition to NO. More specifically, it is the presence of both of these substances that allow the fast reaction to occur, which is also suggested by its formula. This means that when the NO_2/NO_x ratio is around 0.5 all of the NO_x can be handled by the fast reaction. The ideal amount of ammonia for the fast reaction is a 1:1 ratio between ammonia and NO_x . Masaoki and Hirofumi [17], who have studied the phenomenon, attributed stringent adherence to emission regulations to this fast reaction caused by the synergy between the DOC and SCR. They also state that it is difficult to maintain the desired ratio due to changes in the NO_x concentration, flow rate and temperature, and that it is especially difficult at low temperatures due to the DOC not performing its conversion to the same degree.

Figure 2.4 shows NO_x conversion based on temperature and composition. In order to achieve 80% conversion for all compositions, a temperature of 350 °C would have to be maintained, whereas if the composition is around 50% NO_2 temperatures downward of 170 °C are adequate. However, the functionality of the DOC is limited below 200 °C, so it is unlikely to find a scenario where the NO_2/NO_x ratio is 0.5 below such a temperature.

The flow rate of the exhaust gasses affect NO_x conversion in such a way that a higher flow may result in the gasses passing by the catalyst too quickly for a reaction to occur. This effect is often measured using the space velocity of the gas, which is defined as the volumetric flow rate divided by catalyst reactor volume. Baik et al. [8] reported on the effects on NO_x conversion of various space velocities for a Cu-Zeolite catalyst, showing that the largest effects occur at temperatures below 200 °C and increase again above 400-450 °C.

Urea injection and decomposition

Ammonia is a very suitable reactant for reducing NO_x in exhaust gases. Due to its odour, toxicity at high concentrations and boiling point of -33 °C it is hard to handle and store in a mobile application such as a vehicle [16]. Urea, on the other hand, will with ease decompose to ammonia through direct or through multiple reactions. DEF (Diesel Exhaust Fluid) or *AdBlue* consists of 32.5% urea and

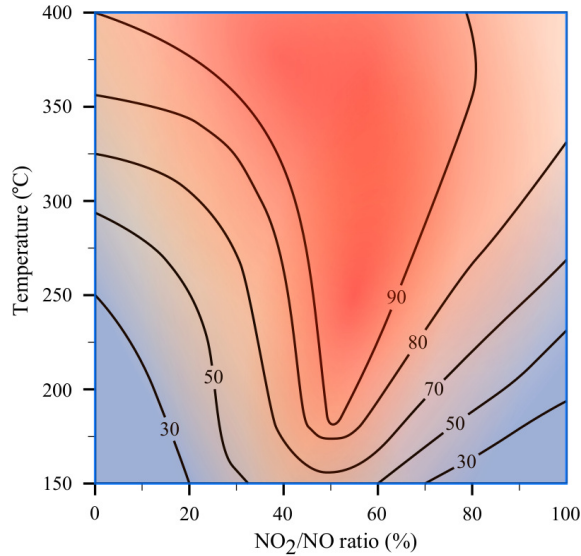
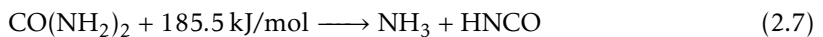


Figure 2.4: Schematic NO_x conversion for different temperatures and compositions using a Fe-Zeolite catalyst. Recreated from data compiled by Masaoki and Hirofumi [17].

67.5% de-ionized water and is most commonly used in automotive applications [3].

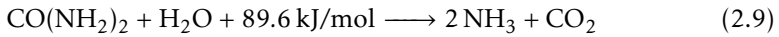
When *AdBlue* ($\text{CO}(\text{NH}_2)_2 + \text{H}_2\text{O}$) is injected into the exhaust gas stream, the water will quickly evaporate due to the high temperatures of the exhaust gas flow, leaving urea ($\text{CO}(\text{NH}_2)_2$). If urea is heated in a slow fashion, decomposition into biuret, triuret, ammonium isocyanate will occur alongside decomposition into ammonia at temperatures ranging from 80 °C to about 180 °C. The ammonia formed by decomposition of urea reacts with the urea itself. Above 180 °C urea may decompose to cyanuric acid or other compounds of higher molecular weight. However, if urea is subject to very fast heating the main reaction occurring is described by Equation (2.7), producing ammonia and isocyanid acid (HNCO). [36]



If urea is not heated fast enough, isocyanid acid from reaction (2.7) may re-

act with urea or even with itself to create aforementioned compounds of higher molecular weight, especially in high temperatures [36]. Isocyanid acid will hydrolyze rapidly according to Equation (2.8) on the surface of any metal oxide, such as V_2O_5 or TiO_2 , that is present in the SCR [9]. Kleemann *et al.* [20] have made an extensive analysis of HNCO decomposition on various catalysts containing various compositions of tungsten (W) and vanadium (V) and they found that there is a sharp decrease in conversion efficiency at temperatures below 180 °C for most catalyst compositions.

In ideal conditions, reaction (2.7) and reaction (2.8) may be carried out simultaneously accordingly to reaction (2.9), only $185.5 - 95.9 = 89.6$ kJ/mol of activation energy will be required for the reaction to occur [36].



There are many difficulties with urea injection as it is hard to predict how much ammonia is required in the SCR for best performance during the acting conditions. Temperature variations will affect the catalysts ability to store ammonia and variations of compositions of the exhausts will effect the reaction processes. Furthermore, too high NH_3/NO_x ratio will lead to ammonia-slip which may lead to increased pollution through N_2O production in the ASC.

2.2.4 Ammonia slip catalyst

In some conditions, the ammonia injected into the exhaust gases will fail to react and bypass the SCR. This is often referred to as ammonia slip. Ammonia has a very strong odor and is irritating on the mucous membrane when exposed to high doses. Ammonia occurs naturally as a fertilizer and will thereby contribute to soil acidification [14].

Fine and ultra fine particle emissions from diesel engine are formed by two modes. Solid soot from the combustion process, ranging from 40 to 150 nm and nucleation mode of more volatile compounds, often smaller than 30 nm. While solid soot is effectively converted to less harmful substances in the DOC and DPF, aerosols formed by nucleation is not considered in legislation and are thereby often neglected [21]. Koronen *et al.* [22] has found that the presence of ammonia in the atmosphere enhances the binary $H_2SO_4 - H_2O$ nucleation rate by several magnitudes. Ammonia emission, however, is legislated for diesel trucks and are therefore considered in the aftertreatment system.

Girard *et al.* [6] have identified three routes to ammonia slip:

- Incomplete SCR reaction (i.e. NO_x conversion efficiency less than NH_3/NO_x ratio from urea injection).
- Release of stored NH_3 from SCR, primarily from a catalyst temperature change affecting catalyst storage capacity.
- Incomplete decomposition of the injected urea upstream the SCR, leading to NH_3 formation in or downstream the SCR.

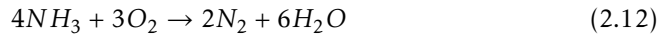
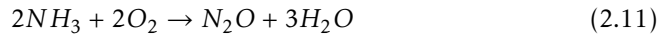
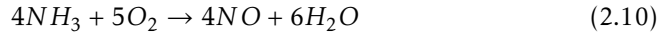
The amount of ammonia required for best deNO_x performance is mostly dependent on temperature, space velocity and composition of the exhaust gases. P.M. Kleeman [19] has found for a $\text{TiO}_2 - \text{WO}_3 - \text{V}_2\text{O}_5$ catalyst that when the ammonia concentration exceeds 20 ppm there is only a slight increase in deNO_x performance. At this point, the SCR reactions (2.4), (2.5) and (2.6) are saturated and the increase of ammonia content will mostly lead to increased ammonia slip.

At exhaust temperatures near but below about 200 °C, the water in the injected urea solution will evaporate, but urea may be left in solid state. The solid urea may be adsorbed on the surface of the catalyst. In a later stage, when the engine is subject to a higher load and the exhaust temperatures rises, the solid urea will decompose into ammonia. At this point, the released ammonia may contribute to a NH_3/NO_x ratio higher than 1, thus resulting in significant ammonia slip. Well tuned urea dosing systems will strive to account for this effect by reducing injected urea during temperature ramps. However, this effect is erratic, making it difficult to compensate for it in a satisfactory matter [38].

Furthermore, urea that already have decomposed into ammonia can be stored on the surface of the SCR catalyst. The catalysts ability to hold ammonia is strongly dependent on temperature. As the temperature increases, the ammonia absorbed on the catalysts decreases. Thus, ammonia is released into the exhaust flow. If not properly taken into account by the urea dosing system, this may lead to a NH_3/NO_x ratio higher than 1 with extensive ammonia slip as a result [38].

While it is possible to enhance the performance of the SCR in terms of NH_3 slip, for instance by reducing injected urea, it often comes to a cost in terms of decreased deNO_x performance. However, by utilizing an ammonia slip catalyst downstream the SCR, the SCR can be tuned for best deNO_x performance, whilst the excessive ammonia is taken care of downstream the SCR in the ASC.

There are three main reactions in the ASC whereas only one is desirable. Equation (2.10) creates NO which counteracts the very benefit of the SCR, thus reducing the net NO_x conversion efficiency. Equation (2.11) produces N_2O , nitrous oxide which is a very potent greenhouse gas. Compared to carbon dioxide, nitrous oxide is approximately 289 times more potent as a greenhouse gas. In addition, N_2O contributes in large extent to stratospheric ozone depletion [37]. The third reaction, equation (2.12) converts the ammonia to nitrogen and water, both harmless. Thus, this reaction is preferred above the others.



In contrast to the SCR catalyst where the amount of ammonia available for reactions can be controlled through the injection of urea, the purpose of the ASC is to handle whatever superfluous ammonia that slips through the SCR. Therefore, the ASC does not have any degrees of freedom except the composition of the catalyst itself. The three reactions (2.10), (2.11) and (2.12) are very similar and as the ASC lacks degrees of freedom, one is unable to tune for best selectivity to nitrogen. However, Hünnekes et al. [38] has found that increased temperature affects the selectivity to nitrogen of the ASC.

2.3 Emission standards

European emission regulations were introduced for heavy-duty trucks in 1992 with EURO I. Since then, several new stages of regulations have been introduced. Since 2013, EURO VI is the acting emission standard in EU [12]. As a result of the stringency of the regulations, truck manufacturers are constantly looking for more efficient engines in terms of energy conversion and minimization of pollution.

EURO VI regulates the amount of harmful residual products forming when burning fuel in the combustion engine. To verify that the engine complies with the regulations, the engine is tested in laboratory environment for both steady-state and transient behaviour as well as off-cycle testing. As of EURO VI, the WHTC (World Harmonized Transient Cycle) and WHTS (World Harmonized Stationary Cycle) which is based on the world-wide pattern of real heavy commercial trucks, is used [12].

Myung *et al.* [31] tested a Daimler AG HD truck for the old and new european test cycles. Myung *et al.* found that the WHTC/WHSC features more realistic driving conditions with lower engine speed and load in rural and urban areas compared to the ETC and ESC. In these regions, the exhaust temperatures were found to be 100–150 °C lower for the WHTC/WHSC. During motorway driving, however, Myung *et al.* found that the WHTC/WHSC features higher torque demand resulting in 100–120 °C higher exhaust temperatures [31]. Hence, the performance of the aftertreatment system is tested in a more widespread area of operation.

The transient driving cycle WHTC consists of a normalized speed and torque map expressed as percentage of maximal engine speed and torque. The specific engine that is to be tested is firstly tested in an engine test cell to construct an

engine map. The WHTC is then denormalized to the specific engine. After an engine map is constructed and the WHTC is denormalized, the engine is forced to cool down to 20–30 °C. A cold start emission test is then performed followed by a hot soak period to ready the engine for the hot start emission test. Lastly, the engine is subject to the full cycle test run. [30]

United States Environmental Protection Agency (EPA) and National Highway Traffic Safety Administration (NHTSA) have jointly adopted a so called "Phase 2" program that promotes a new generation of greener trucks in terms of fuel efficiency and thereby CO₂ emission [1]. The program stretches to year 2027 and aims to include the effect of technologies not yet exploited in determining the expected fuel consumption reduction. Up to 25% fuel reduction is expected on class 7 and class 8 combination tractors and a up to 9% reduction is expected for trailers. Enhancing aerodynamics, reducing rolling resistance and weight reduction is identified as some of the areas that needs to be addressed in order to achieve the CO₂ reduction expected. For the engine itself, an up to 5% reduction of CO₂ emission is expected. Reduced internal friction, waste heat recovery and improved emissions aftertreatment are identified as some of the areas of possible improvement.

3

Optimization environment

The optimization environment developed in this thesis consists of several different parts. The HEV is modeled by a diesel engine, NO_x maps, electric motor loss map, a battery pack and an aftertreatment system. No complete vehicle model is used since the propulsion and corresponding emissions are the main interest. All of the models are described further in Section 3.5. CasADi [40] reformulates the models into symbolic ones. YOP [25] then uses the symbolic models in the creation of an optimal control problem (OCP), containing initial and final values, constraints and cost function etc. The OCP along with a simulated initial guess is used to create a nonlinear problem (NLP). IPOPT [39], which is described in its documentation as an open source software package for large-scale nonlinear optimization, is then used to solve the NLP. For further information about these external packages the reader is referred to their respective documentations. A visualization of the optimization process is displayed in Figure 3.1.

3.1 Development procedure

At the start of the thesis an example case exists for optimal tip-in using only the diesel engine. This case investigates the controls to quickest achieve steady-state conditions after a step in engine load. The engine operates at a fixed specified speed throughout the experiment, which is insufficient for the purposes of this thesis. The main alterations required are integration of the additional models (electric motor and aftertreatment system) and implementing the capability of following a specified drive cycle. The cost function can easily be adapted to suit whatever case is desired. The model is expanded incrementally and each added feature is tested and verified before the next feature is piled on. This is to decrease the difficulty of debugging.

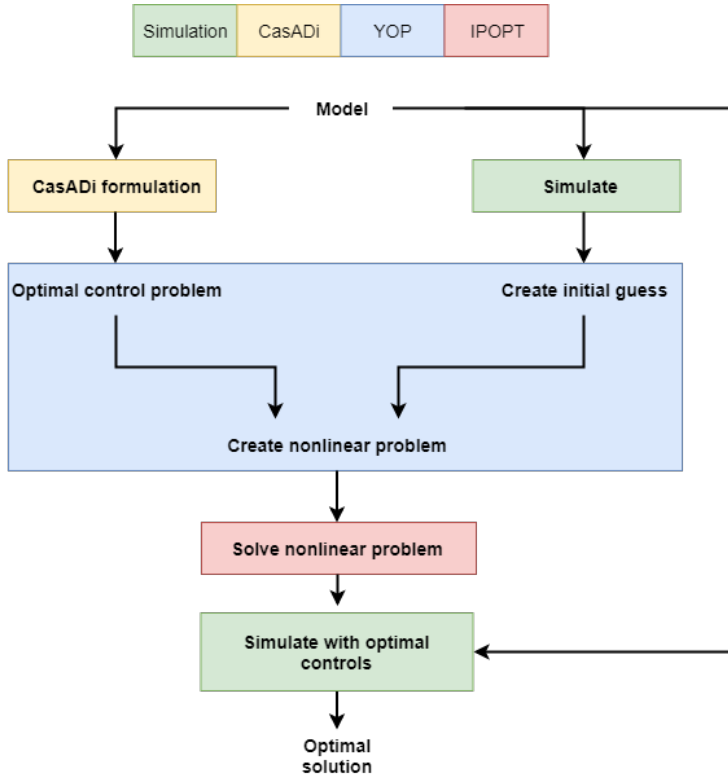


Figure 3.1: Visualization of the optimization environment and process. The models are used both in formulating an optimal control problem, simulating to acquire an initial guess and finally simulating using the optimal controls.

3.2 Lookup tables

To be able to define a non-linear problem (NLP) using YOP, the model must be continuously differentiable. Therefore, there must be no logic expressions or other discontinuous operations within the model. To be able to include, for example, efficiency and NO_x maps in the model formulations, the CasADi function `casadi.interpolant` is used to create lookup tables for all discontinuities and maps.

Very finely gridded lookup tables are demanding for the NLP solver and increases the duration of each iteration in the optimization. Furthermore, a finely gridded lookup table takes a long time to create. Therefore, the lookup tables are designed so as to receive acceptable performance whilst keeping the complexity low. Lookup tables are created for the following applications:

- Electric motor power loss map
- NO_x map
- WHTC engine speed profile
- WHTC engine acceleration profile
- WHTC engine torque profile

The electric motor power loss map was given for equally spaced values of electric motor speed and output torque. The data is smooth and continuous which enables the lookup table to be created from very few data points whilst providing the required accuracy.

The lookup table for the WHTC engine speed profile is created from equally spaced data points four times denser than the original data made by linear interpolation. The acceleration profile is created from finite differentiation of the speed profile and this data is also four times denser than the original data.

The torque profile is erratic and occasionally jumps from a high torque value to a negative torque from one point to the next. Therefore, it is harder to approximate the profile with the *casadi.interpolant* function. The original data for the torque profile consists of one torque value per second. Using an extremely dense equally spaced grid to capture the behavior is not an option as too much computational power is required to handle the resulting interpolant function. Still, densely situated data points are required at every original data point since large ripples will occur otherwise, see Figure (3.2). To account for this while keeping the interpolant function minimal, four data points in each direction from an original point is linearly interpolated, see Figure (3.3). This way, the resulting interpolant function is minimal but accurate and without large ripples around data points where the derivative changes as can be seen in Figure (3.3).

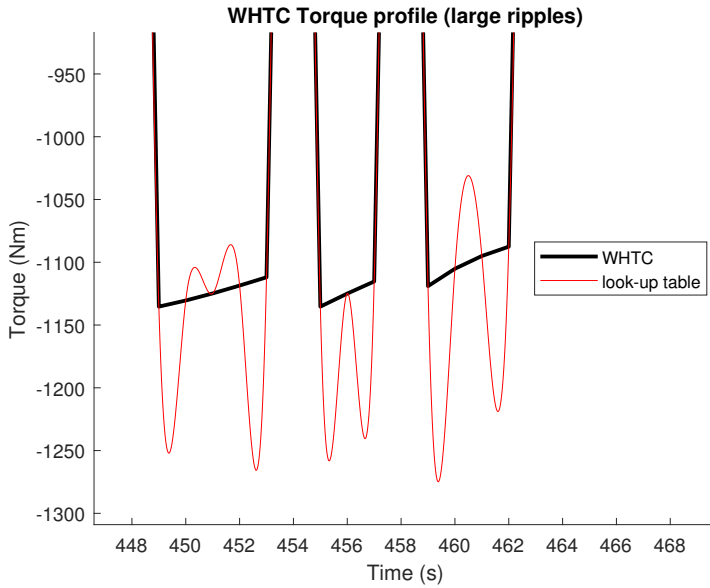


Figure 3.2: Ripples occur if the interpolated data is too sparse.

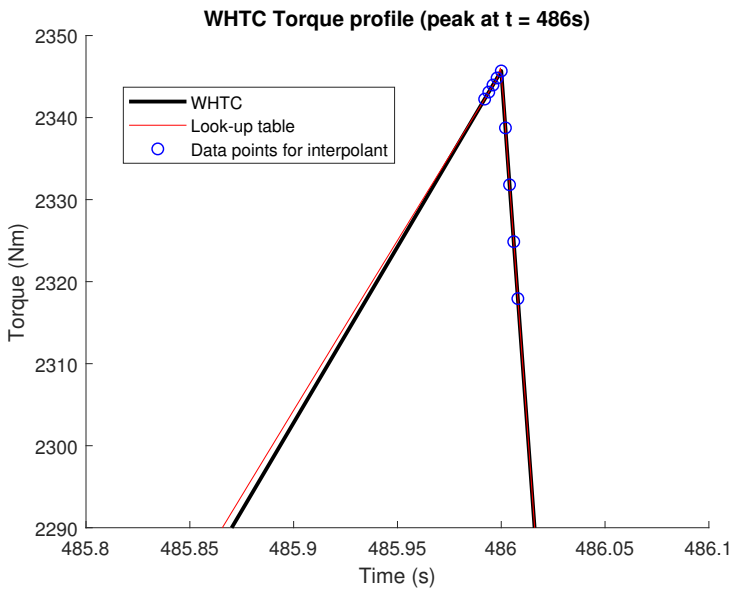


Figure 3.3: Four points in each direction from the original WHTC torque data point at $t = 486$ s are linearly interpolated. Red curve is the resulting lookup table.

3.3 Denormalization of WHTC

WHTC is a normalized driving cycle designed to be adapted to each individual engine, as previously described in section 2.3. The engine speed and torque profile of WHTC is formulated as normalized percentage values that needs to be denormalized for the specific engine. This denormalization is performed in Appendix A under the assumption that the electric motor is utilizing 1000 Nm of torque during engine braking.

3.4 Solver initial guess

YOP requires an initial guess on the control signal vector as well as an initial guess on the state vector. This initial guess is utilized in the solver in the first iteration and every iteration is made by a step from the previous iteration. Also, the solver may go back to an earlier iteration if it finds bad solutions (complex numbers etc.) or if the objective function is not decreased during the last iteration. Therefore, a good initial guess will enable the solver to find the optimal solution faster and easier. Furthermore, for a non-convex problem an initial guess close to the optimal solution may be necessary for convergence of the solver.

As the state vector largely depends on the control signals through the dynamics of the model, the initial guess of the state vector is obtained through simulation of a guessed control vector. For a conventional engine, the initial guess on fuel injection can be done with good accuracy using a simple linear scaling and offset of the torque demand due to the strong correlation between the fuel injected and the shaft torque. For the throttle and wastegate control signals, it is more difficult to estimate the behavior throughout the cycle. Therefore, the wastegate is assumed closed and the throttle opened.

3.5 Model description

The model is controlled in a piecewise linear manner, where the pieces are, for example, the collocation intervals when using direct collocation. The linearity comes from keeping the derivative of the control signals constant, as opposed to the more common piecewise constant case where the control signals themselves are kept constant. This provides smoother transitions between intervals since the control signals remain continuous. Furthermore, using linear control signals in the optimization is more realistic than constant controls for each interval. See Figure 3.4 for an illustration.

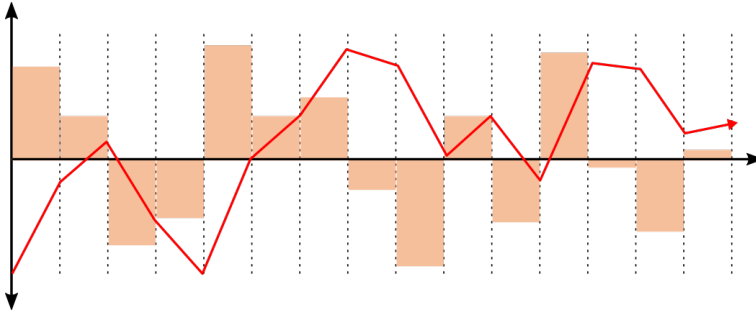


Figure 3.4: Schematic plot of the piece-wise constant derivative of the control signal for each time interval in bars and the piece-wise linear control signals in solid red.

3.5.1 Electric motor

The electric motor has a maximum power of 155 kW and a maximum speed of 3000 rpm. It can deliver a maximum torque of 1500 Nm at motor speeds below about 1000 rpm. Above 1000 rpm, the maximum torque decreases as the maximum power is achieved and kept constant as the motor speed increases, see Figure 3.5. The motor is assumed to be mounted in line with the engine, thus, the motor speed will equal the engine speed and no mechanical losses in transmission from the electric motor will be modelled. However, mechanical losses and electrical losses are present throughout the operating range of the electric machine as can be seen in Figure 3.6.

The constraints on the maximum torque is modelled using two independent functions. The first is linear and will limit the torque in regions below 1000 rpm, where the torque is not to exceed 1500 Nm. The other one is a third order polynomial, which catches the behaviour of the decreasing torque at increasing motor speeds. In Figure 3.7 the four blue curves represent the individual constraints on motor torque and the red dotted curve is the maximum torque.

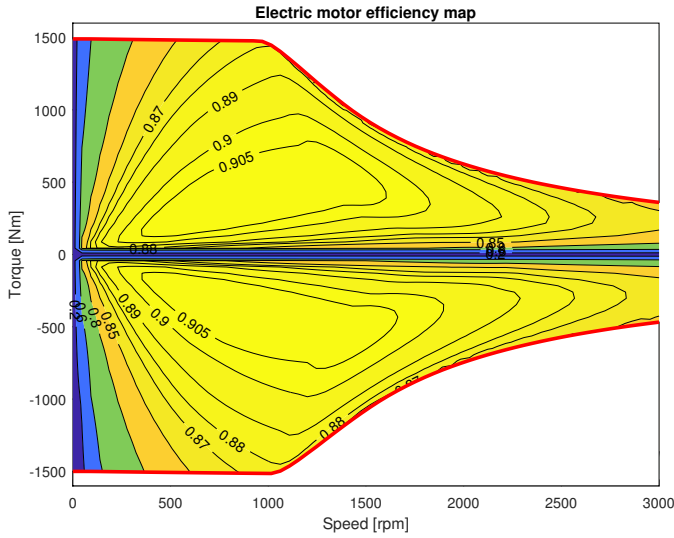


Figure 3.5: Map of electric motor efficiency in different operating points. The red line marks torque limit up to around 1050 rpm and power limit thereafter.

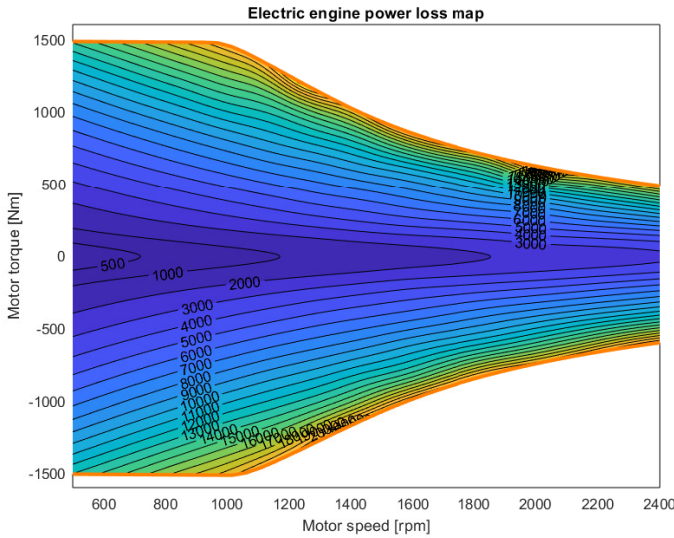


Figure 3.6: Map of electric motor power losses (W) in different operating points. The orange line marks torque limit up to around 1050 rpm and power limit thereafter.

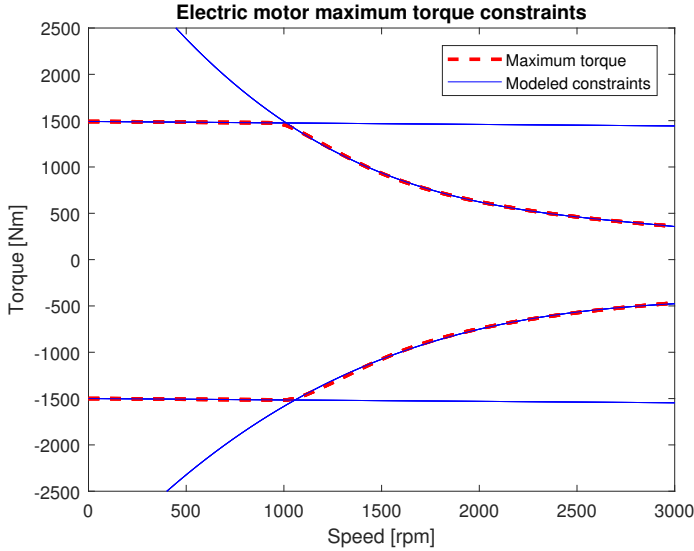


Figure 3.7: Lines and third order polynomials (blue) used to model limit on torque (red).

3.5.2 Battery

The battery for the truck is made out of several LiFePO_4 cells. Data for a single specific cell includes capacity, nominal voltage and voltages corresponding to seven state of charge values, among with other data. The nominal voltage of each cell is 3.3 V, the capacity is 2.3 Ah and the cell can deliver and receive a maximum of 35 A. High currents are related to high resistive losses which can be seen by combining Ohm's law with Joule's law, resulting in equation (3.1).

$$P = R \cdot I^2 \quad (3.1)$$

A high battery voltage is preferred as the current required for a specific power output decreases with increasing battery voltage according to Ohm's law. However, increasing the battery voltage increases the required number of series connected cells. For Li-ion batteries, each series cell pack needs to be balanced for their voltages not to drift from each other during repetitive charge and discharge cycling. A battery monitoring system (BMS) does just that. However, a BMS becomes more expensive and complex as more cell packs are configured in series, which is why it is also of value to limit the number of series connections (even though the battery pack is assumed to be balanced in the model). The nominal battery voltage is chosen to 650.1 V, which corresponds to 197 series cells.

The battery is dimensioned to be able to handle the maximum power request from the electric motor which occurs at an engine speed of 1154 rpm. The max-

imum torque produced at this engine speed is 1301 Nm with a conversion efficiency of 87.64%, resulting in a required electrical power of 179.4 kW and a delivered mechanical power of 157.2 kW. With a nominal battery voltage of 650.1 V, the required current is approximately 276 A. Each cell can deliver up to 35 A, thus, a minimum of 8 parallel cells in each series pack is required. With this configuration the capacity of the battery is 18.4 Ah or about 12 kWh.

The SOC vs. open circuit voltage (U_{oc}) will be used in the optimization to extract U_{oc} given the value of state of charge. Therefore, it is crucial that the state of charge can be seamlessly converted to open circuit voltage throughout the usable SOC range of the battery. This is done by utilizing a ‘‘Piecewise Cubic Hermite Interpolating Polynomial’’, ‘pchip’ in Matlab. The result of this interpolation can be seen as the solid blue curve in Figure 3.8.

The SOC vs U_{oc} can be approximated by a cubic polynomial function from SOC-values ranging from 0.2 to 0.8, equation (3.2), which later can be used in the optimal control parser. Above and below this interval, the battery is subject to rapid voltage increase/decrease for changing SOC values, thus, these areas are avoided. Storing LiFePO₄ batteries at high SOC will decrease their lifetime [2], emphasizing the importance of not overcharging the battery and of storing the cells at a moderate charge level. Furthermore, J. R. Belt et al. [29] has found that increased SOC span during battery cycle testing increases the aging of the battery. Therefore, the SOC of the battery is chosen to be kept between 25% and 50% as indicated by the green area in Figure 3.8. Thus, the usable capacity of the battery is approximately 4 kWh. Due to the high charging power capacity of the cells, the battery will fully charge in about 80 seconds during extreme conditions. This means that the battery will be able to fully discharge/charge during relatively short driving missions.

$$U_{oc} = 115.91 \cdot (SOC)^3 - 183.11 \cdot (SOC)^2 + 110.17 \cdot (SOC) + 634.46 \text{ V} \quad (3.2)$$

3.5.3 Diesel engine

For the engine, the LiU-diesel 2 [24] model was used. Unlike the first LiU-diesel it does not have exhaust gas recirculation or variable geometry turbine. The standard model has four states, to which states for NO_x and engine speed has been added for a total of six states:

- Charge air cooler pressure
- Intake manifold pressure
- Exhaust manifold pressure
- Turbocharger angular velocity

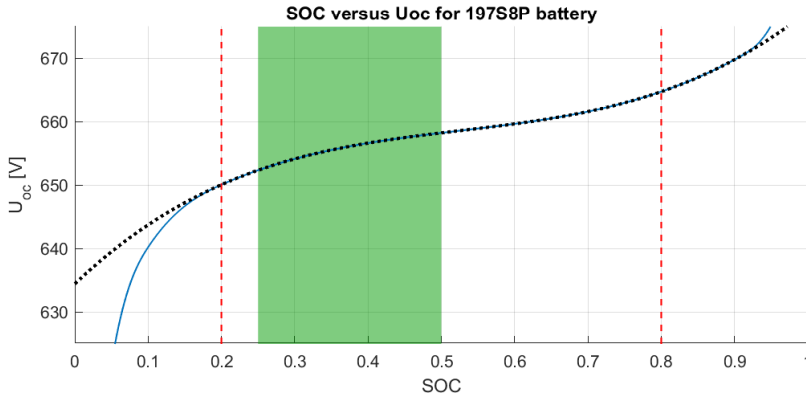


Figure 3.8: Open circuit voltage as a function of state of charge. Red dotted lines indicates the limits to the fitting of the polynomial in Equation (3.2). Solid blue curve is the interpolation of the seven data points given and the dotted black curve is the fitted polynomial. Green area indicates the SOC range that will be used.

- Engine out NO_x
- Engine speed

The engine out NO_x state is required both for direct inspection of the emissions and for passing along the values to the aftertreatment model. The state works as an integrator so that NO_x accumulates over time. While the temperature dynamics of the exhaust system are slow, the out-of-engine NO_x is assumed to travel from the engine to the SCR catalyst instantaneously. Thus, no extra state for NO_x is required for each component in the exhaust system.

Engine speed is added as a state in the engine model. Since the desired driving cycle is known, the dynamics of the state can be described by finite differences of the speed profile of a drive cycle. These differences are interpolated for resolution and stored in a CasADi lookup table. This way, only an initial value for the engine speed needs to be specified and the derivative at any given time is fetched from the table.

The use of the lookup table for the dynamics leads to significant drift in engine speed, as shown in Figure 3.9. This is because, while the table is indeed continuous, only one value is fetched for the given time and used for the entire discretization interval. This is corrected by implementing a proportional feedback on the derivative, with the error function as the difference between the speed at the given time (also retrieved from a CasADi lookup table) and the current value of the engine speed state as seen in Equation (3.3).

$$dN = dN_{lut} + k_p \cdot (N_{lut} - N) \quad (3.3)$$

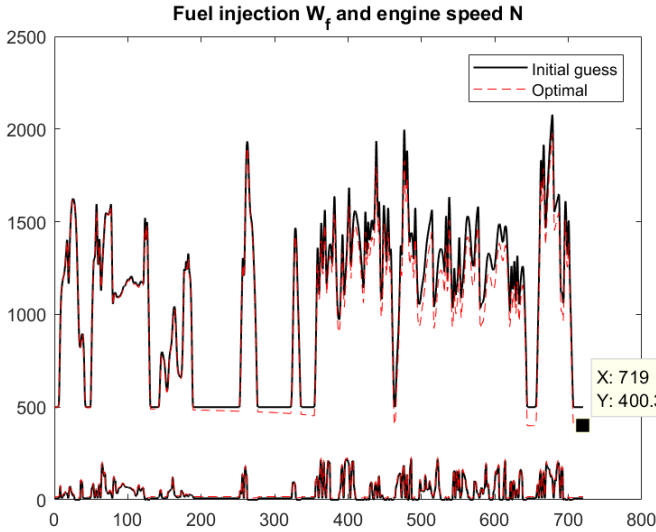


Figure 3.9: Engine speed for the first 720 seconds of WHTC and corresponding guess for fuel injection trajectory (black) in comparison to drifting values acquired from a lookup table without the use of a feedback (red). The showcased drift in engine speed, seen as the difference between red and black curves, causes the optimization to fail 720 seconds into the 1800 second cycle.

The standard controls for this model are unchanged:

- Fuel injection
- Throttle position
- Wastegate position

Engine-out NO_x

The NO_x emissions from the engine may be of interest when, for instance, assessing the performance of the aftertreatment system. By comparing the exhaust that leaves the engine with those that exit at the tailpipe, the effect of the aftertreatment can be seen. The engine-out NO_x produced during combustion is modeled with the use of a lookup table based on a NO_x map. The map is illustrated in Figure 3.10.

The map is extrapolated below the friction torque curve to ensure that no negative NO_x values occur. While maximum torque is modeled in the LiU Diesel 2

engine model, the minimum torque (from friction) was found by fitting a second order polynomial to friction data acquired through iterative simulation of the model. The extrapolation of the map is done based on points that are selected in order to give a slightly generalized and smoothed result.

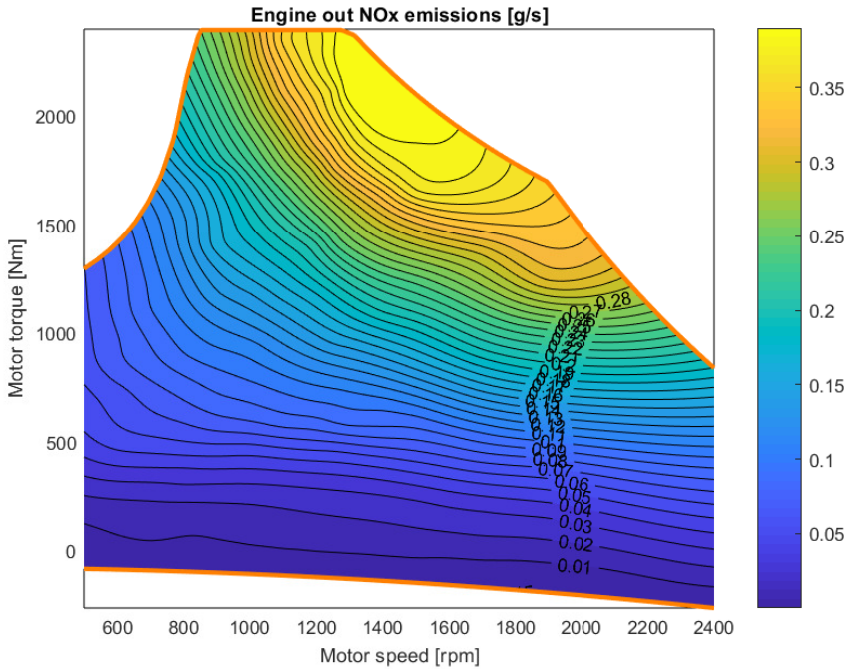


Figure 3.10: Emission map for NO_x with engine operating region marked in orange. The negative lower limit describes the friction torque when no fuel is injected. The largest values are present when most fuel is injected, i.e. at the maximum power.

3.5.4 Aftertreatment system

The exhaust aftertreatment system (EATS) model consists of a DOC, DPF and SCR, and is fed with exhaust manifold temperature and mass flow from the engine model. The components of the system are split into segments, each of which contain a state for temperature. The DOC has two segments (and thus two states), the DPF has three, and the SCR has five segments and states. The temperature of the last segment of the DOC is equal to the first temperature in the DPF, and the last temperature in the DPF is equal to the first of the SCR.

Validation of the model is performed by comparing its output to measurement

data from a WHTC cycle performed with an unrelated engine and aftertreatment system. Since the model is unrelated to the measurement data the validation is not absolute, but rather serves as an indication of realistic behavior. Worth noting is that the modeled temperature after the turbine/wastegate is fed directly to the EATS whereas the measured input temperature is likely performed closer to the DOC, resulting in differing input temperatures. This is compensated for by scaling the modeled DOC until the subsequent modeled temperatures present similar behavior as their corresponding measurements. No measurement is available for the temperature after the SCR. The modeled and measured temperatures are shown in Figure 3.11. As can be seen, the model captures most of the measured behavior. An apparent difference is that of the initial values, which is due to the modeled case using cold start temperatures of 20 °C.

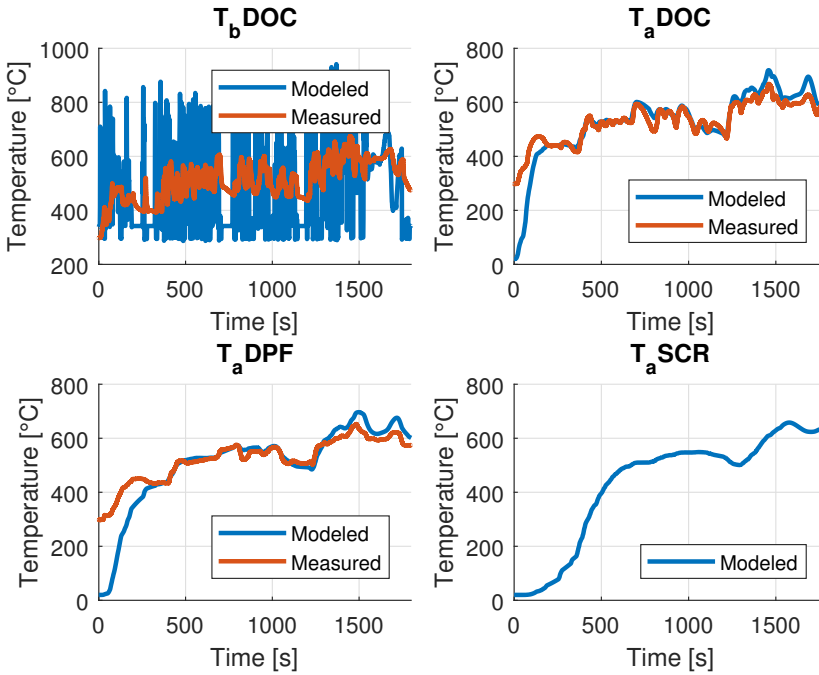


Figure 3.11: Temperatures of the aftertreatment system. Despite the differing input temperatures seen in the first figure, scaling of the DOC leads to model behavior similar to the measurements, as shown in the second and third figure. Indices “a” and “b” stands for after and before.

The SCR temperature dictates deNO_x performance. Since the SCR consists of five segments, it also has five temperatures. This raises the question of what temperature to base deNO_x performance on. An illustration of the temperatures in the individual segments of the SCR over the WHTC cycle is shown in Figure 3.12.

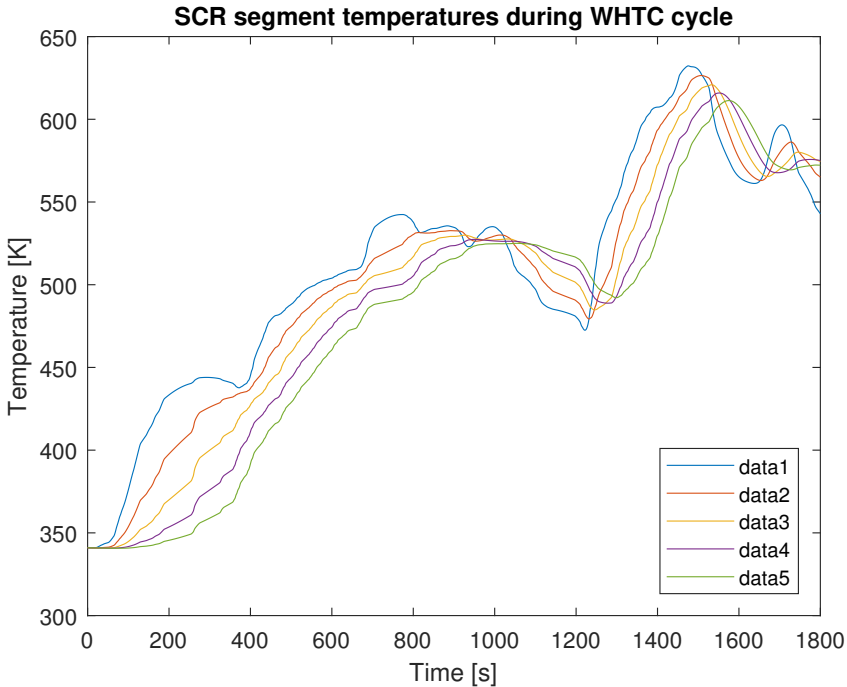


Figure 3.12: Temperatures of the five SCR model segments for the WHTC cycle, where *data1* is the first segment.

While it is possible to construct a mean temperature from the five segments, Figure 3.12 indicates that the temperature in the middle (third) segment is located between the temperatures of the surrounding segments. Thus, the third segment is selected to determine deNO_x activity.

The effect of temperature on SCR activity also depends on the catalyst substance. The most common variants in the automotive field are copper zeolite (Cu-Zeolite) and iron zeolite (Fe-Zeolite), where Cu-Zeolite generally has a lower light-off temperature, but Fe-Zeolite has better deNO_x performance at high temperatures. Since the examined powertrain and aftertreatment system is not based on a vehicle that exists in reality, there is no reason to limit the investigation to only one of the two. Instead, a deNO_x model is created for each of the two catalyst variants and the SCR temperature is fed to both of them, so that their respective performance for a given scenario can be put directly in contrast to one another. The deNO_x models are based on experiments performed by Guan *et. al.* [26], and are shown in Figure 3.13.

In order to ensure predictable asymptotic behavior of the model curves, they are

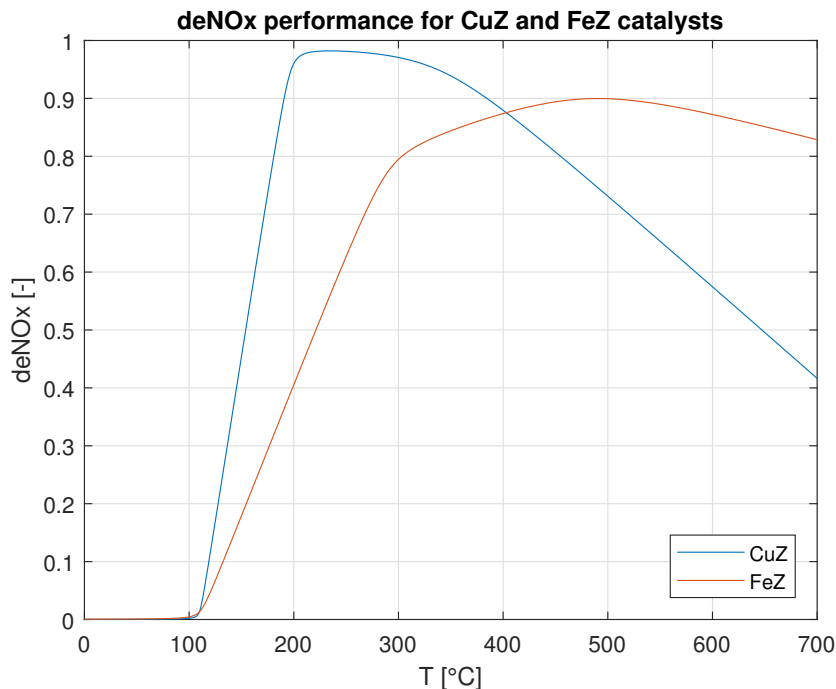


Figure 3.13: Modeled Cu-Zeolite and Fe-Zeolite catalyst activity with respect to temperature.

constructed using four separate lines instead of using a fitted polynomial, see Figure 3.14. Also worth noting is that in the experiments on which the curves are based [26], the maximum tested temperature was about 600 °C. This means that above 600 °C the deNO_x performance is extrapolated, although since the WHTC cycle seldom elicits such high temperatures in the SCR, this is not considered a problem.

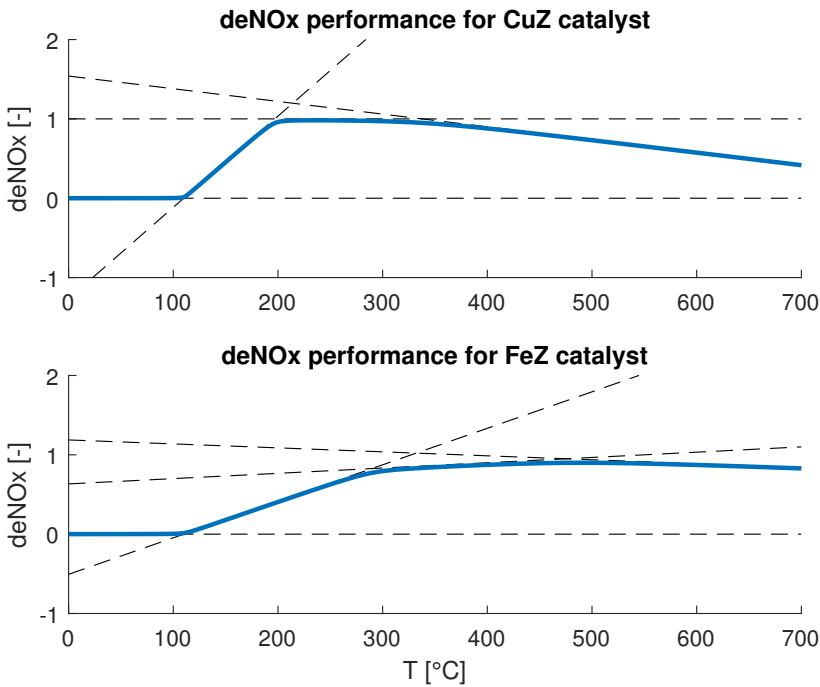


Figure 3.14: Construction of the $deNO_x$ curves for Cu-Zeolite and Fe-Zeolite catalysts.

3.6 Optimization limitations

The optimization environment is unable to handle the throttle as a free variable, possibly due to the resulting complexity. However, it is possible to manually set the throttle to a constant value for the experiment. In this way it is possible to compare the solutions for different throttle values for specific cases to examine the effect of closing the throttle. This is specifically interesting for cases where the exhaust system is subject to rapid heating.

The case of complete shutdown of the conventional engine is not investigated as this requires complex modelling of the start-up behavior. Therefore, there are always pumping losses and friction present within the combustion engine and the electric motor. The minimum engine speed is set to 500 rpm.

4

Results

In this chapter several cases are investigated and optimized for best performance according to the objective for the specific experiment. The results are analyzed and discussed. Mainly three subdivisions are devised for examination: contrasts in temperatures and emissions for hybrid and conventional powertrain for the WHTC, optimal control of cold engine with respect to NO_x , and trade-off between optimal control for NO_x and fuel.

4.1 WHTC temperature and deNOx comparison

Conventional	Hybrid
$\min_u \int_0^{1800} W_f(t, u) dt$	$\min_u \int_0^{1800} W_f(t, u) dt$
$s.t. \quad M_{ice}(t) + M_{em}(t) = M_{whtc}(t)$ $N(t) = N_{whtc}(t)$	$s.t. \quad 0.25 \leq SOC(t) \leq 0.5$ $SOC(t_{end}) \geq 0.375$ $SOC(t_0) = 0.375$ $M_{ice}(t) + M_{em}(t) = M_{whtc}(t)$ $N(t) = N_{whtc}(t)$

One hypothesis on which this thesis is based is that the engine and aftertreatment temperatures may sometimes be lower for the HEV than for the conventional driveline, and that this causes difficulties maintaining deNOx activity in the SCR. This is tested using the WHTC cycle. The length of the experiment is determined by the cycle, which is 1800 seconds. The objective is to minimize the fuel mass-

flow (W_f).

While the available models provide numerous combinations of vehicle configurations and optimization parameters that can be compared against one another, certain objective functions prove difficult for the optimizer to minimize, making some data hard to acquire. Thus, the temperatures and NO_x emissions of the HEV and conventional driveline are compared in the case of a WHTC cycle which is optimized for fuel efficiency. Minimizing NO_x over WHTC is not possible for either configuration. This is likely due to NO_x being more difficult to control than fuel consumption, which corresponds directly to the fuel injection control signal. An interesting case for comparison is therefore left unexplored.

The temperature after the turbine and wastegate is used to emulate the engine out temperature, as this is the final temperature of the engine model and the one that is fed into the aftertreatment system. This temperature for both the conventional and hybrid case can be seen in Figure 4.1, along with moving means to illustrate their differences more clearly. The moving mean temperature of the HEV is consistently 25–50 °C lower than that of the conventional configuration. Overall, the peaks are higher and there is a larger variation in the temperatures from the conventional powertrain than from the hybrid.

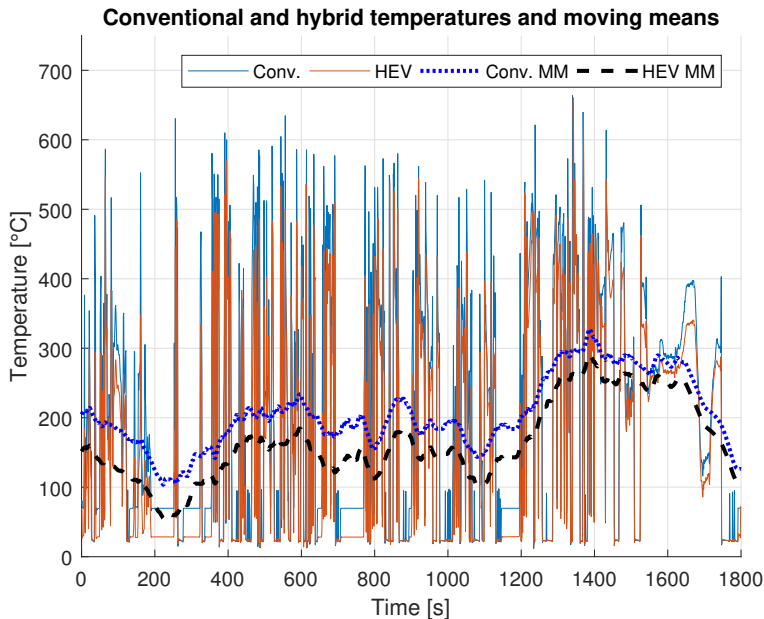


Figure 4.1: Temperature after turbine/wastegate for the conventional and hybrid drivelines, as well as their respective moving means (MM) during a WHTC cycle optimized for fuel efficiency.

Figure 4.1 does not divulge how often each temperature occurs. Therefore, the temperature distribution for the same case is shown in Figure 4.2. The most frequent temperatures for both conventional and HEV configurations are found in the lower range between 0 and 100 °C, represented by the tallest bars in Figure 4.2. One obvious difference between the configurations is that the conventional one has a higher idling temperature than the HEV. This is due to engine speed being fixed by the WHTC cycle, and the conventional vehicle thus consumes some fuel in order to overcome pumping and friction losses, whereas this is performed by the electric motor in the HEV. The coldest temperatures occur during engine braking and are the same for both configurations. This suggests that the light-off temperature of the SCR likely plays a large role in deNO_x performance.

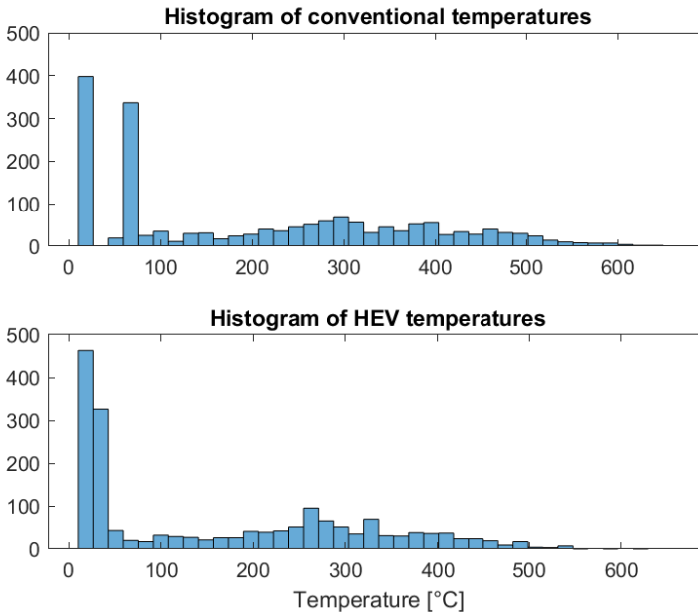


Figure 4.2: Number of occurrences of Conventional and HEV temperatures. The values are divided into 40 bins, resulting in each bin spanning approximately 16 °C. The tallest bar can be attributed to engine braking and the second tallest to idling.

The resulting SCR temperatures are shown in Figure 4.3. The HEV temperature is lower than the conventional one, which is consistent with the temperatures entering the aftertreatment system. These are the temperatures that are used to determine the deNO_x activity described in Figure 3.13.

Supplying the SCR temperatures to the deNO_x curves yields the deNO_x activity

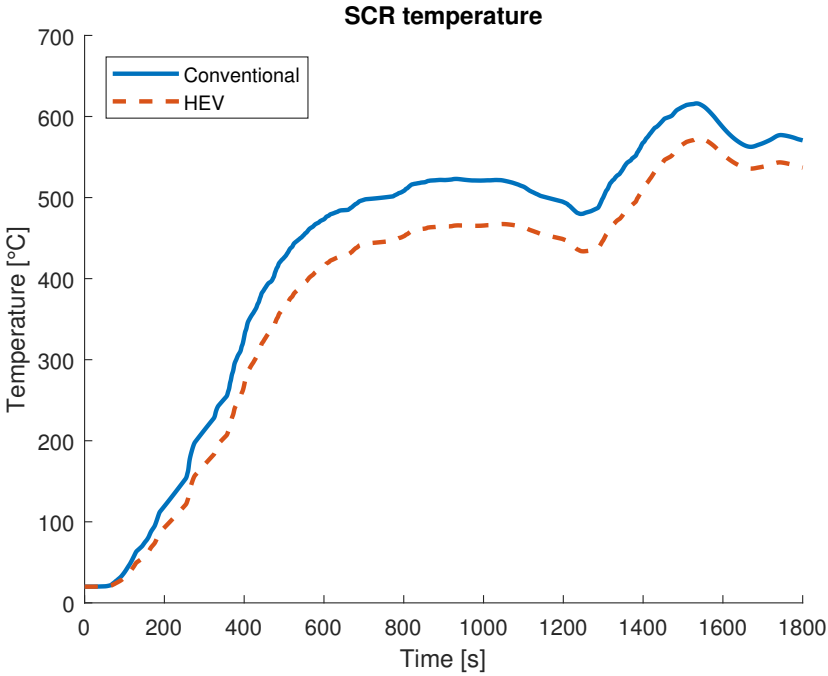


Figure 4.3: SCR temperature of conventional and HEV powertrains during fuel optimal WHTC.

at each point of the cycle. This allows comparison of Cu-Zeolite and Fe-Zeolite catalysts for the same scenario. Figure 4.4 shows the deNO_x performance for the different combinations of powertrain and catalyst.

It is apparent that the Cu-Zeolite catalyst lights off faster than the Fe-Zeolite for both the conventional and hybrid powertrains. However, Cu-Zeolite activity drops rapidly after reaching its maximum due to the increasing temperature, with the hybrid maintaining higher performance than its conventional counterpart due to its lower temperature. Meanwhile, the Fe-Zeolite catalyst activity stays close to its maximum for the remainder of the cycle, with no apparent difference between the conventional and hybrid powertrains.

The deNO_x performance and engine out NO_x can be used to calculate tailpipe NO_x . In Figure 4.5 and Table 4.1, the engine out and tailpipe emissions for the catalysts and powertrain configurations are compared. It is clear that the hybrid powertrain yields less engine-out NO_x , and that the Fe-Zeolite catalyst performs better than the Cu-Zeolite catalyst for both configurations.

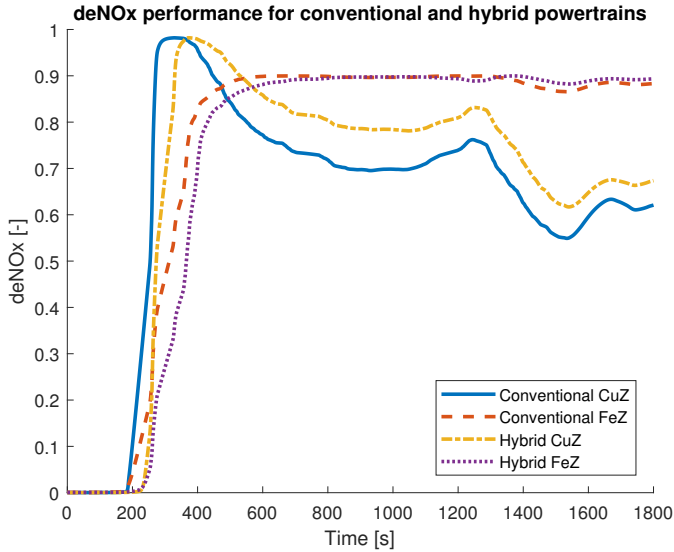


Figure 4.4: Conventional and HEV deNO_x activity with Cu-Zeolite and Fe-Zeolite catalysts. The Cu-Zeolite catalyst lights off faster but its performance is hampered due to high temperatures later in the cycle. The Fe-Zeolite catalyst lights off slower but maintains its performance at higher temperatures.

Table 4.1: Engine out and tailpipe NO_x for hybrid and conventional drive-lines using Cu-Zeolite and Fe-Zeolite catalysts, with deNO_x performance in parenthesis.

	EO NO _x (g)	CuZ NO _x (g)	FeZ NO _x (g)
Conventional	159.43	54.33 (66%)	26.39 (83%)
HEV	112.60	31.07 (72%)	18.41 (83%)

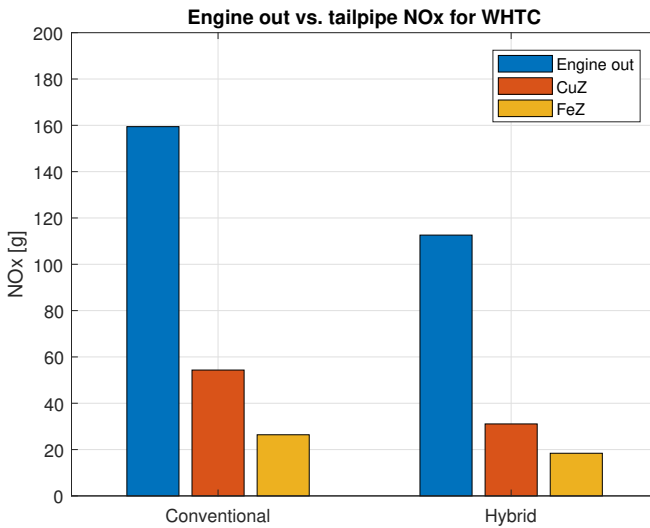


Figure 4.5: NO_x emissions for different powertrain and catalyst combinations. The HEV emits less NO_x than the conventional. Both catalysts provide significant NO_x reduction, but the Fe-Zeolite catalyst has a higher reduction for both configurations.

4.2 Optimal control for cold start

During cold starts the aftertreatment system does not work as intended. As a consequence, more emissions are released until the aftertreatment system is of adequate temperature. The aftertreatment system consists of a series of components with their respective masses and heat transfer to the surroundings. Therefore, it takes time for the components in the aftertreatment system to absorb enough heat to reach the activation temperature of the catalyst.

The ability to utilize the hybrid powertrain to quickly heat up the exhaust system for a swift light-off of the SCR is investigated. The objective of this problem is to minimize the time it takes for the catalyst to light-off, i.e. for the center-most segment of the SCR to reach 200 °C from an initial temperature of 20 °C. The state of charge is allowed to move freely during the optimization. It is also investigated if such measures are beneficial in terms of NO_x emissions and fuel consumption.

Two steady-state cases are investigated for optimal cold start control, one more demanding operating point and one close to idling. The demanding operating point consists of a constant output torque of 800 Nm at an engine speed of 1100 rpm. The close to idling operating point is at 550 rpm and 250 Nm of output torque. Both cases are investigated for a hybrid powertrain and a conventional powertrain for comparison of the two. The initial temperatures of the components in the exhaust system are set to 20 °C.

Not all variations of powertrain setups can be analyzed due to limitations in the optimizations. Throttling may be used to decrease the flow through the engine, thus increasing the pumping work, resulting in lower efficiency and more heat for warming the aftertreatment system. Even though the results of such action cannot be investigated, general conclusions can be derived from the optimal controls for the cases investigated.

4.2.1 High load operating point

In steady-state operation at a net torque output of 800 Nm and engine speed of 1100 rpm, the fastest possible light-off of the SCR catalyst is investigated for both the hybrid and conventional powertrain. Optimal NO_x performance for both Cu-Zeolite and Fe-Zeolite catalyst is also analyzed for both configurations.

Conventional - minimized light-off time

$$\min_u t_{end}$$

$$\begin{aligned} \text{s.t.} \quad & T_{SCR3}(t_{end}) \geq 200 \text{ }^\circ\text{C} \\ & M_{ice}(t) + M_{em}(t) = 800 \text{ Nm} \\ & N(t) = 1100 \text{ rpm} \end{aligned}$$

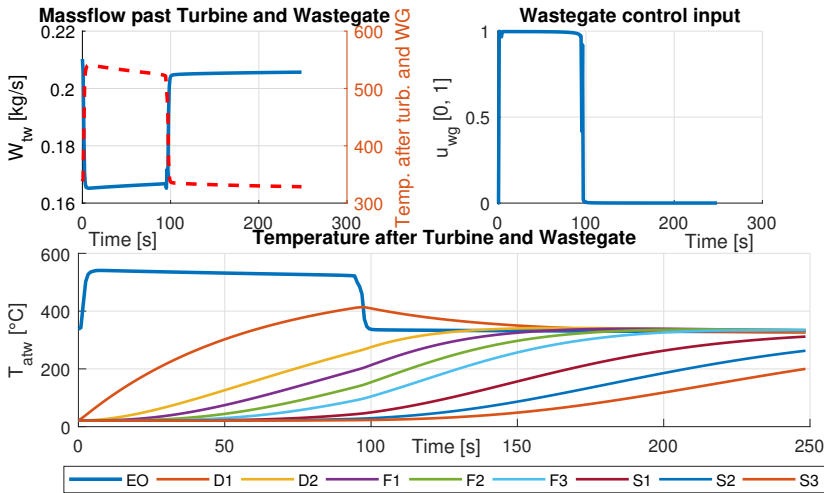


Figure 4.6: Conventional powertrain during steady state operation at 1100 rpm and 800 Nm optimized for fastest activation of the SCR. 249 seconds is required to reach 200 °C in the mid-segment of the SCR (S3). “EO” is the engine-out temperature, “D” is the DOC (2 segments), “F” the DPF (3 segments) and “S” stands for SCR. The SCR have 5 segments, but only the first 3 are displayed.

The optimal light-off behavior for the conventional powertrain consists of two phases. In the first phase the wastegate is fully opened ($u_{wg} = 1$) in order to disable the turbocharger and limit the flow through the engine. The temperature entering the exhaust system is thereby very high as can be seen in Figure 4.6. After approximately 95 seconds the powertrain enters the next phase. The wastegate is abruptly closed to enable turbocharging and the flow through the engine increases as the turbocharger is spooling up. At this point, the heat previously built up in the first mode is pushed through the exhaust system to faster reach the SCR. It takes 249 seconds for the catalyst to light-off.

Hybrid - minimized light-off time

$$\min_u t_{end}$$

$$\begin{aligned} \text{s.t.} \quad & 0.25 \leq SOC(t) \leq 0.5 \\ & SOC(t_{end}) \geq 0.375 \\ & SOC(t_0) = 0.375 \\ & T_{SCR3}(t_{end}) \geq 200 \text{ } ^\circ\text{C} \\ & M_{ice}(t) + M_{em}(t) = 800 \text{ Nm} \\ & N(t) = 1100 \text{ rpm} \end{aligned}$$

The hybrid powertrain exhibits the same wastegate behavior as the conventional powertrain, with an opened wastegate initially to later be closed as can be seen in Figure 4.7. However, the ability to increase engine load and charge the battery is utilized, thus, making the heating phase shorter than for the conventional case.

Additional loading of the diesel engine results in much higher temperatures as more fuel is injected. The fuel consumption and emissions increases but the light-off of the SCR is accelerated. However, not all of the extra energy from the additional fuel can be stored in the battery as some is lost in conversion to chemical energy. Figure 4.8 shows the optimal state of charge and the optimal torque split between the combustion engine and the electric motor.

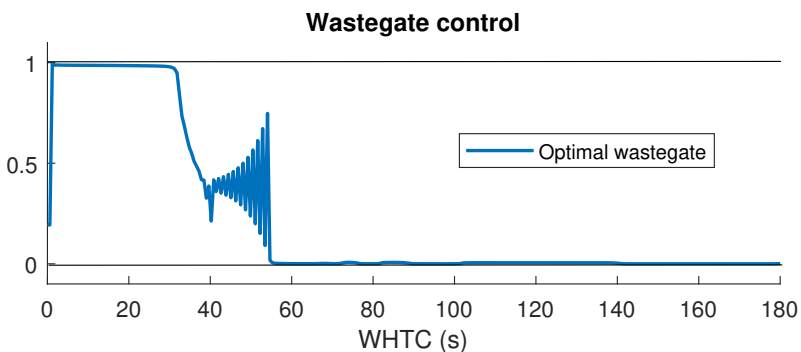


Figure 4.7: Wastegate control for fastest catalyst light-off for a hybrid configuration during steady-state conditions at 800 Nm output torque at 1100 rpm.

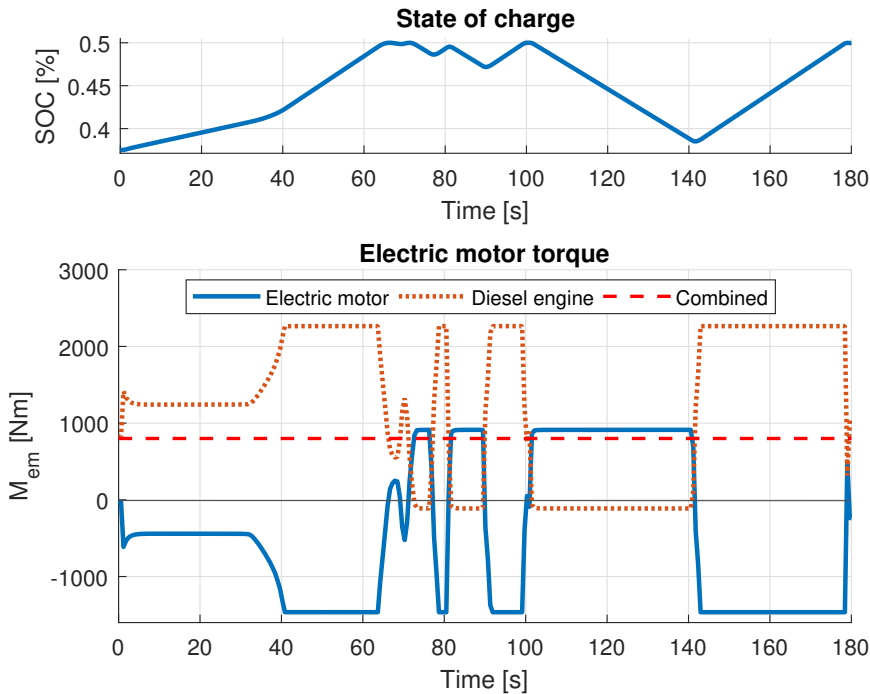


Figure 4.8: State of charge and torque of the hybrid configuration when minimizing light-off time during steady-state conditions at 800 Nm output torque at 1100 rpm.

Hybrid - Optimal control for minimum NO_x emission with Cu-Zeolite catalyst

$$\min_u \int_0^{1200} \text{NO}_x \, dt$$

$$\begin{aligned} \text{s.t.} \quad & 0.25 \leq \text{SOC}(t) \leq 0.5 \\ & \text{SOC}(t_{\text{end}}) \geq 0.375 \\ & \text{SOC}(t_0) = 0.375 \\ & M_{\text{ice}}(t) + M_{\text{em}}(t) = 800 \, \text{Nm} \\ & N(t) = 1100 \, \text{rpm} \end{aligned}$$

Instead of minimizing the lightoff time, NO_x is minimized instead. Thus, the end time of the experiment has to be specified. 1200 seconds provides ample time to observe the temperature dynamics of the aftertreatment system. The upper plot in Figure 4.9 shows the torque distribution between the combustion engine and the electric motor. During the first minute of the run the combustion engine is heavily loaded by charging the battery. Initially the wastegate is fully open in the

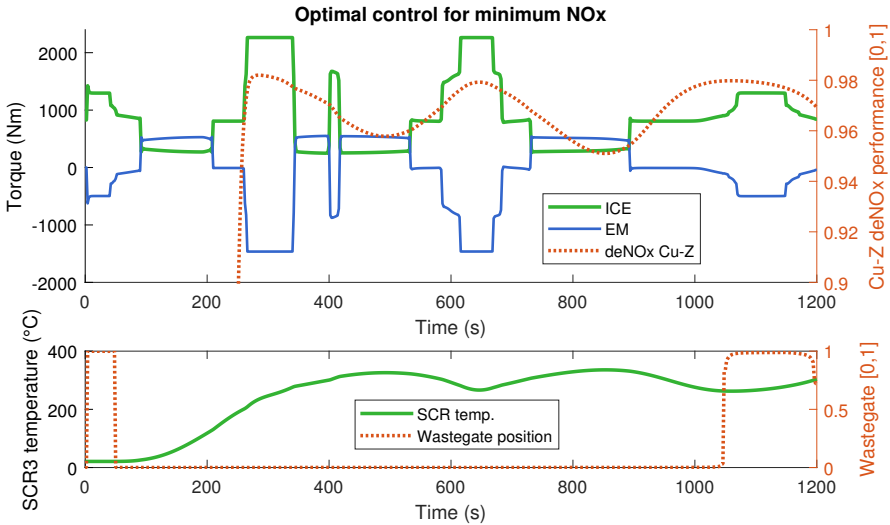


Figure 4.9: The hybrid configuration is controlled for minimized NO_x with respect to a Cu-Zeolite catalyst during steady-state driving at 250 Nm output torque and 550 rpm. The top plot shows how deNO_x performance pulses along with ICE torque. The bottom plot shows SCR temperature and a wastegate that is closed for most of the run.

same manner as for the previous cases to enable fast heating of the exhaust system. As enough heat has been produced the combustion engine starts to almost idle with very little output torque, supported by the electric machine to produce the required torque output.

Once the heat produced in the early stage has travelled to the SCR catalyst and the temperature reaches 200 °C, the deNO_x performance increases drastically. The peaking deNO_x performance is taken advantage of by the combustion engine as it is producing as much torque as the electric motor can handle, plus the output torque.

As the temperature increases the deNO_x performance is reduced due to the characteristics of the Cu-Zeolite catalyst. When the deNO_x performance decreases the combustion engine is once again put in a close to idling operating point to reduce the out-of engine NO_x , supported by the electric machine to deliver the required torque. Once the temperature has dropped enough for the catalyst to attain its best performance the combustion engine once again delivers as much torque as the electric powertrain can absorb. The temperature distribution can be seen in Figure 4.10.

The pulsing in the use of the combustion engine is a recurring behavior ob-

tained for several runs tested for the hybrid configuration controlled for minimal NO_x emission. While this behavior is optimal for minimizing NO_x emission, it is not optimal in terms of fuel efficiency. Optimizing for fuel efficiency results in 5.9749 kg of used fuel, while 6.4910 kg of fuel is used when minimizing for NO_x emission, an increase of 8.64%. The NO_x emission, however, is reduced with 23.25% when optimizing for NO_x emission.

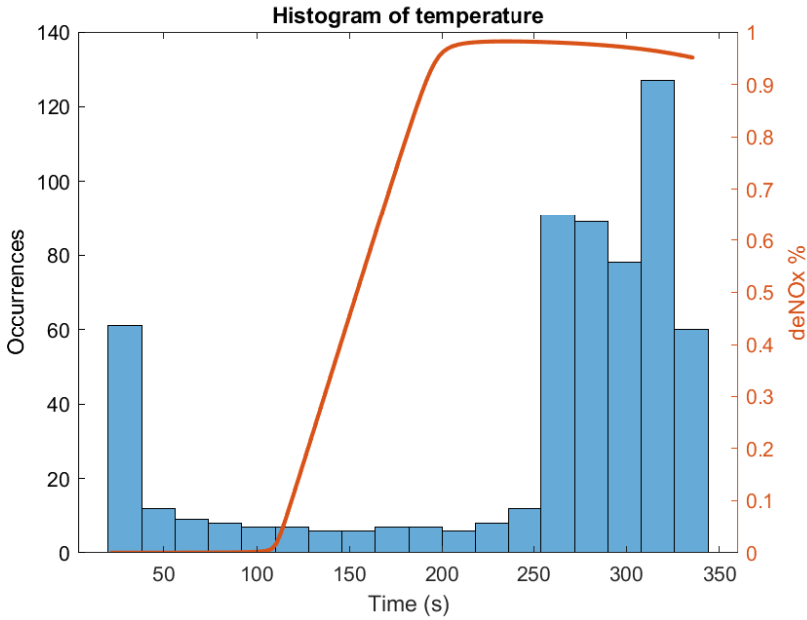


Figure 4.10: Temperature distribution and deNO_x performance. The hybrid is optimized for minimum NO_x with respect to a Cu-Zeolite catalyst at a steady-state operating point of 250 Nm and 550 rpm.

Hybrid - Optimal control for minimum NO_x emission with Fe-Zeolite catalyst

$$\min_u \int_0^{1200} \text{NO}_x \, dt$$

$$\begin{aligned} \text{s.t.} \quad & 0.25 \leq \text{SOC}(t) \leq 0.5 \\ & \text{SOC}(t_{\text{end}}) \geq 0.375 \\ & \text{SOC}(t_0) = 0.375 \\ & M_{\text{ice}}(t) + M_{\text{em}}(t) = 800 \text{ Nm} \\ & N(t) = 1100 \text{ rpm} \end{aligned}$$

The best deNO_x performance for the Fe-Zeolite catalyst is at around 480 °C, which is apprehended in the SCR from about 800 seconds and forth, Figure 4.11. To be able to produce this temperature, the wastegate is somewhat open during the significant part of the run. In the beginning of the run the wastegate exhibit the same behavior as previously described to increase the heating process of the SCR catalyst.

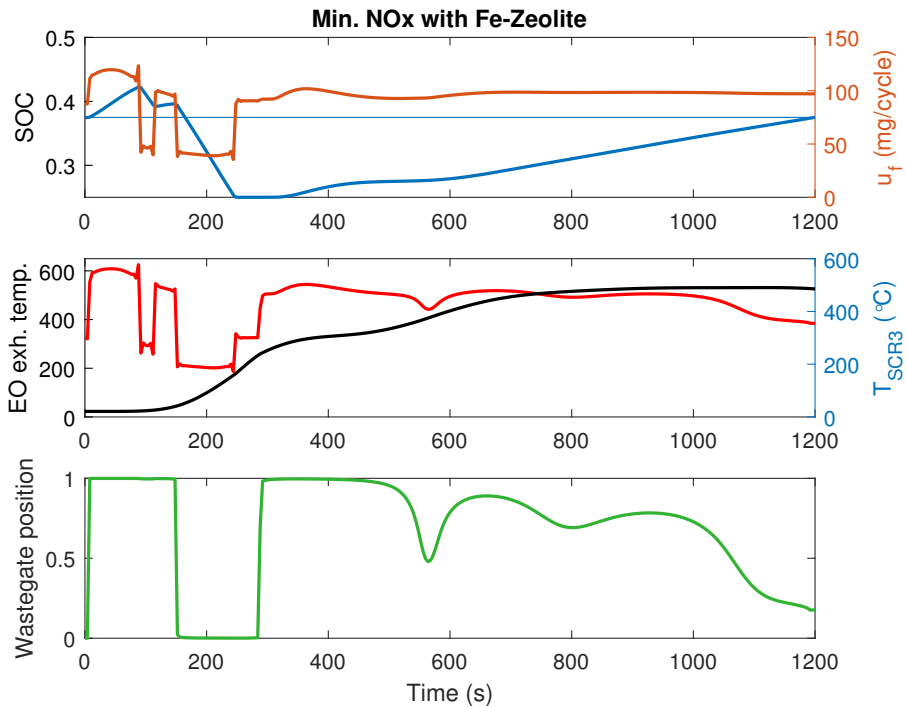


Figure 4.11: Steady-state conditions for hybrid powertrain with Fe-Zeolite catalyst optimized for minimum NO_x emission.

Comparison for high load operating point

Figure 4.13 shows a 20 minute run for four cases. In two cases, one hybrid and one conventional, the powertrain is controlled for optimal light-off until the mid-segment of the SCR catalyst reaches 200 °C. Then, once the SCR is activated, the powertrain is controlled for optimal fuel efficiency for the rest of the run. For the hybrid case, it takes 180 seconds for the catalyst to light-off and for the optimal control objective to change. 249 seconds is required for the conventional powertrain. The third case is a hybrid configuration controlled throughout the run for minimum out-of-pipe NO_x emission in the case of Cu-Zeolite catalyst. The fourth case is a hybrid configuration controlled for minimum out-of-pipe NO_x through

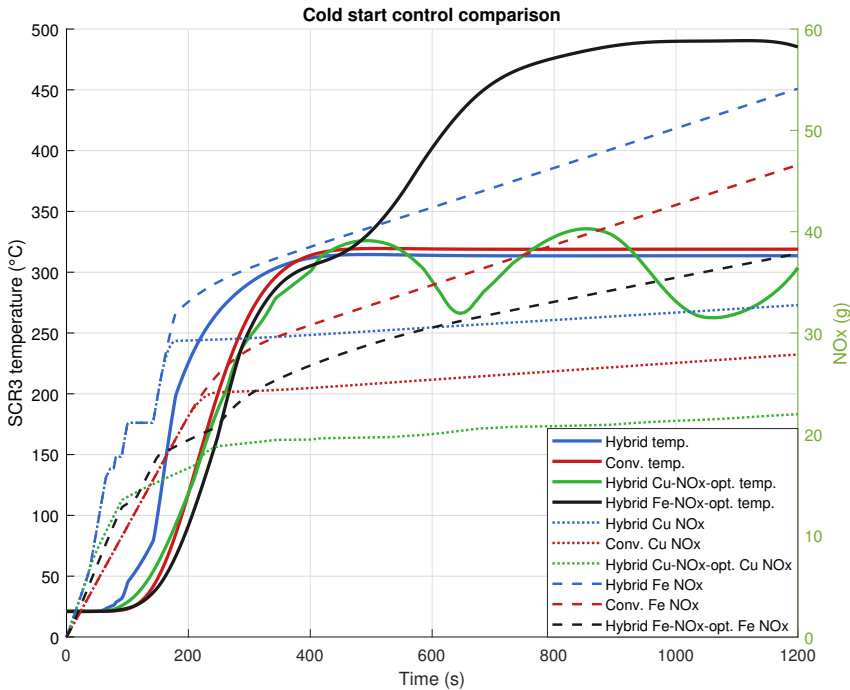


Figure 4.13: Steady state conditions at 1100 rpm and 800 Nm output torque. The hybrid (red) and the conventional powertrain (blue) is controlled for fastest heat-up of the third segment of the SCR catalyst. When the temperature has reached 200 °C the powertrain is controlled for optimal fuel efficiency for the rest of the run. The hybrid in green is controlled for minimum tailpipe NO_x emission for the case of Cu-Zeolite catalyst for the whole 1200 seconds run. The hybrid in black is controlled for minimum tailpipe NO_x for a Fe-Zeolite catalyst.

deNO_x performance at these relative low temperatures. The accumulated values are presented in Table 4.2.

The hybrid powertrain controlled for minimum tailpipe NO_x emission exhibits the highest temperatures as the deNO_x performance for the Fe-Zeolite catalyst peaks at approximately 480 °C. The other cases (apart from Cu-Zeolite NO_x optimal case) strive to put the engine in an operating point with low out-of-engine NO_x emission, as soon as the catalyst is activated. Therefore, the SCR catalyst temperature is lower for these cases.

Table 4.2 presents the achieved results for the examined cases. The conventional powertrain is the most fuel efficient and the hybrid configuration with Cu-Zeolite

catalyst controlled for minimal NO_x consumes the most fuel. However, this case emits the least NO_x emission compared to both Fe-Zeolite catalyst and other cases examined.

Table 4.2: Cold start experiment during steady-state operation at 1100 rpm and 800 Nm for several powertrain configurations for comparison.

Experiment	Wastegate	Throttle	Light-off time (s)	Fuel consumed (g)	Cu NO_x emissions (g)	Fe NO_x emissions (g)	Consumed energy (MJ)
Hybrid	×		180	6179	32.75	54.11	265.06
Conventional	×		249	5937	27.88	46.60	254.69
Hybrid Cu-Z NO_x -opt.	×		260	6491	21.98	-	278.46
Hybrid Fe-Z NO_x -opt.	×		268	6118	-	37.84	262.47

4.2.2 Low load operating point

The experiments performed at the high operating point in Section 4.2.1 are repeated for a different operating point close to idling. A steady-state case with 250 Nm of output torque at 550 rpm is investigated for a cold engine. All initial temperatures of the exhaust system components are set to 20 °C and the objective function to minimize is the time it takes for the mid-segment of the SCR to reach 200 °C.

At this operating point the conventional configuration is able to activate the catalyst. If less output torque is to be delivered the conventional powertrain will struggle to achieve the adequate temperature for the catalyst to light-off. Because of the ability to further load the conventional engine by charging the battery, the hybrid configurations do not suffer from the same limitations.

Conventional - minimized light-off time

$$\min_u t_{end}$$

$$\begin{aligned} \text{s.t.} \quad & T_{SCR3}(t_{end}) \geq 200 \text{ °C} \\ & M_{ice}(t) + M_{em}(t) = 250 \text{ Nm} \\ & N(t) = 550 \text{ rpm} \end{aligned}$$

In the same manner as for the demanding operating point the conventional engine cycles through two phases. The first phase is heating with the wastegate fully open to limit the massflow through the engine. When enough heat is generated the wastegate is closed and the heat is pushed through the exhaust system as the turbocharger is increasing the massflow through the engine.

Due to the low output torque to be delivered the conventional engine struggles to reach the activation temperature of the catalyst. It takes 1114 seconds for the catalyst to light-off.

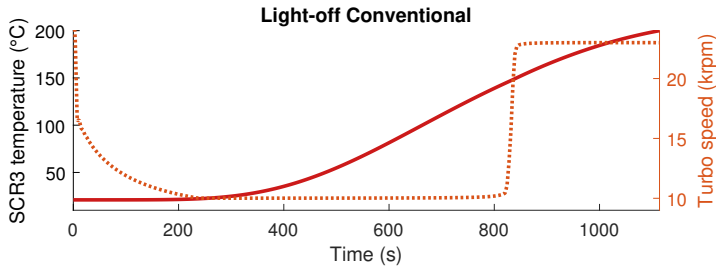


Figure 4.14: Mid-segment temperature of the SCR and the turbocharger speed for the conventional powertrain for fastest activation of the catalyst. 1114 seconds is required for the mid-segment of the SCR to reach 200 °C. At about 830 seconds the wastegate is closed, enabling the turbocharger to speed up to increase the massflow through the engine.

Hybrid - minimized light-off time

$$\min_u \quad t_{end}$$

$$\begin{aligned} s.t. \quad & 0.25 \leq SOC(t) \leq 0.5 \\ & SOC(t_{end}) \geq 0.375 \\ & SOC(t_0) = 0.375 \\ & T_{SCR3}(t_{end}) \geq 200 \text{ }^\circ\text{C} \\ & M_{ice}(t) + M_{em}(t) = 250 \text{ Nm} \\ & N(t) = 550 \text{ rpm} \end{aligned}$$

The same wastegate behavior can be observed for the hybrid configuration. Due to the ability to additionally load the combustion energy by charging the battery the activation of the catalyst is accelerated. It takes 648 seconds for the catalyst to light-off and the battery is fully charged as the catalyst activates. Due to the rapid charging, the battery is fully charged in approximately 2 minutes at the beginning of the run as can be seen in Figure 4.15.

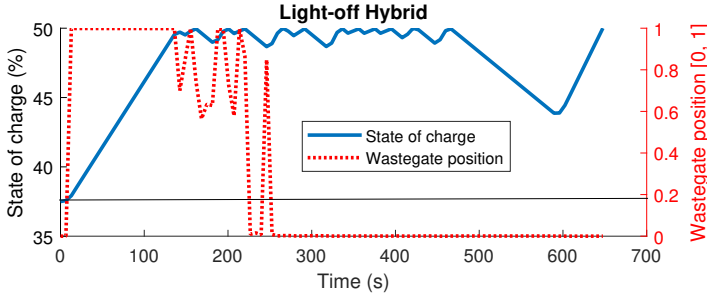


Figure 4.15: State of charge and wastegate position for fastest possible activation of the Cu-Zeolite catalyst during steady-state conditions.

Hybrid - Optimal control for minimum NO_x emission with Cu-Zeolite catalyst

$$\min_u \int_0^{1114} \text{NO}_x \, dt$$

$$\begin{aligned} \text{s.t.} \quad & 0.25 \leq \text{SOC}(t) \leq 0.5 \\ & \text{SOC}(t_{\text{end}}) \geq 0.375 \\ & \text{SOC}(t_0) = 0.375 \\ & M_{\text{ice}}(t) + M_{\text{em}}(t) = 250 \text{ Nm} \\ & N(t) = 550 \text{ rpm} \end{aligned}$$

The objective in this case is not to heat the catalyst in the fastest manner possible, but to optimize 1114 seconds steady-state driving for minimized NO_x emissions, see Figure 4.16. 1114 seconds is chosen because it is the time it takes for the conventional powertrain to heat the catalyst, thus, they are easily comparable.

At the beginning of the run the maximum torque available at 550 rpm is produced by the combustion engine and the battery is charged with the excessive power produced. The wastegate does not exhibit the same behavior as apprehended in the other cases, but is closed during all sessions with heavy loading of the combustion engine. It may be that the amount of power produced cannot be apprehended without the works of the turbocharger, thus the wastegate must be closed. During periods of light loading of the combustion engine the wastegate is opened. Disabling the turbocharging of the engine decreases the massflow and less fuel is required to sustain a high exhaust temperature, which may the objective during the phases of light-loading. The temperature occurrences can be seen in Figure 4.17.

About 120 seconds in, the electric motor starts to produce a small percentage of the requested torque. The out-of-engine exhaust temperature at this point is about 200 °C. This behavior lasts until 400 seconds have passed. At this point

the internal combustion engine is shut down and the electric motor produces the required torque. The engine speed is constantly 550 rpm even though no fuel is injected. Thus, there is still a massflow through the engine, transporting the heat through the exhaust system.

As the exhaust system has a high thermal inertia the temperature in the SCR catalyst steadily increases even though the combustion engine is coasting. As the temperature in the SCR catalyst approaches 200 °C, the deNO_x performance increases drastically which is taken to advantage by the combustion engine. Once again, the maximum available power is produced by the combustion engine, but this time, barely any NO_x is released as the deNO_x performance is at its peak, as can be seen in the lower plot in Figure 4.16.

It seems like the optimizer is taking advantage of the thermal inertia in the exhaust system and pulsing the output power of the combustion engine in sync with the best deNO_x performance. In the lower plot of Figure 4.16 the accumulated NO_x can be seen barely increasing from 700 to 900 seconds even though the combustion engine is heavily loaded due to the exceptional deNO_x performance. Most of the NO_x emissions are generated in the first phase of warming as the catalyst has not yet activated and the combustion engine is heavily loaded.

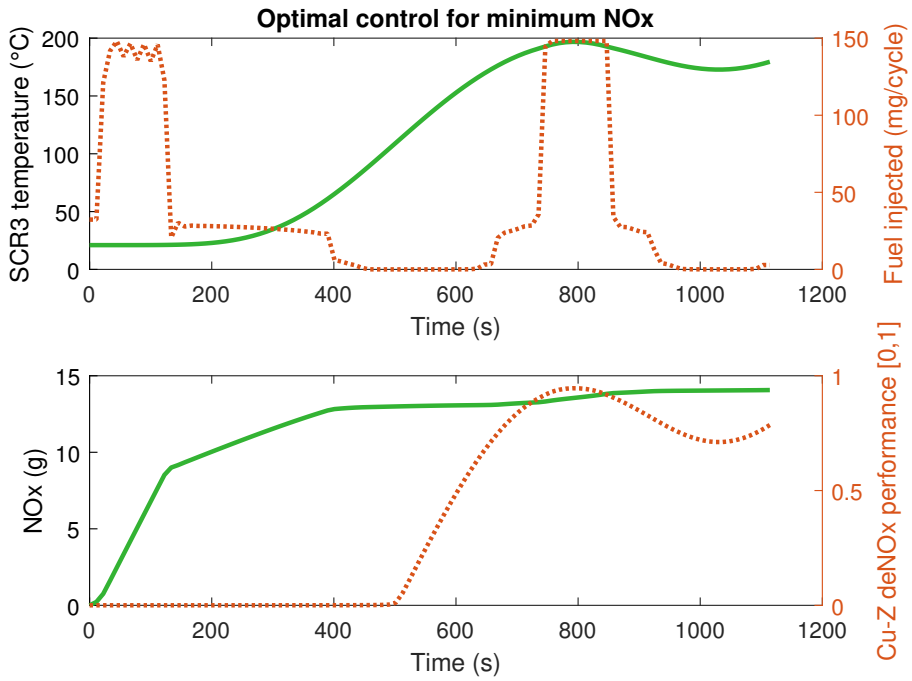


Figure 4.16: Optimal controls for minimizing NO_x emissions during steady-state driving conditions with 250 Nm of output torque at 550 rpm.

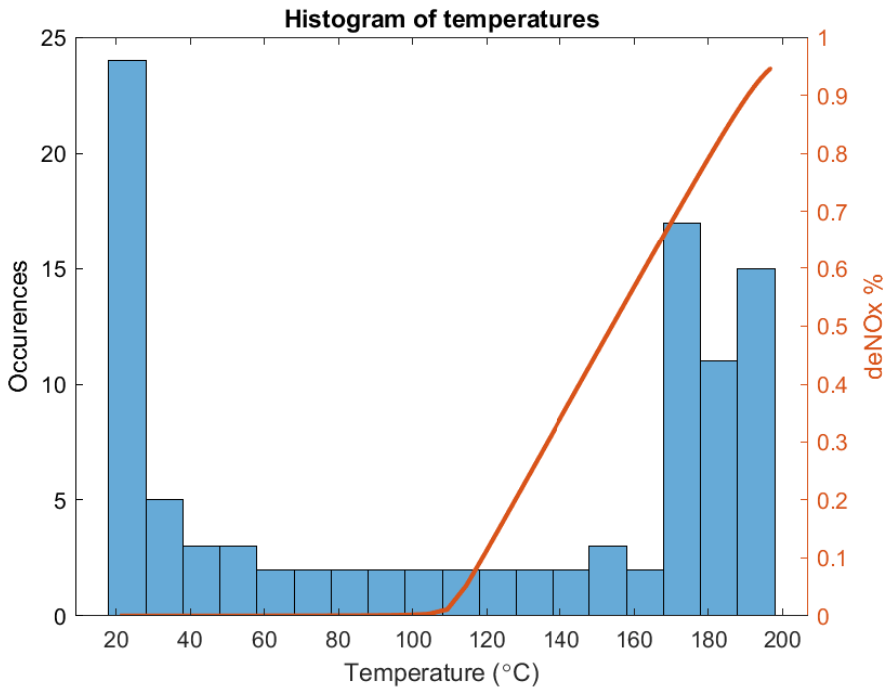


Figure 4.17: Histogram of temperature occurrences and deNO_x performance.

Hybrid - Optimal control for minimum NO_x emission with Fe-Zeolite catalyst

$$\min_u \int_0^{1114} \text{NO}_x \, dt$$

$$\begin{aligned} \text{s.t.} \quad & 0.25 \leq \text{SOC}(t) \leq 0.5 \\ & \text{SOC}(t_{\text{end}}) \geq 0.375 \\ & \text{SOC}(t_0) = 0.375 \\ & M_{\text{ice}}(t) + M_{\text{em}}(t) = 250 \text{ Nm} \\ & N(t) = 550 \text{ rpm} \end{aligned}$$

When controlling the powertrain for minimization of NO_x with a Fe-Zeolite catalyst it is not NO_x efficient heating the exhaust gases by loading the engine more than necessary. However, until approximately 700 seconds have past, the wastegate is open, disabling the works of the turbocharger, thereby increasing the exhaust gases. Due to this behavior it takes very long time until the catalysts activates. The temperature in the mid-segment of the SCR only reaches approximately 180 °C during the 1114 seconds optimized.

During the run the battery is slowly drained as the electric motor is producing torque. At the end of the run when the deNO_x performance is as high as it gets during the run, the battery is charged to make up for the lost energy.

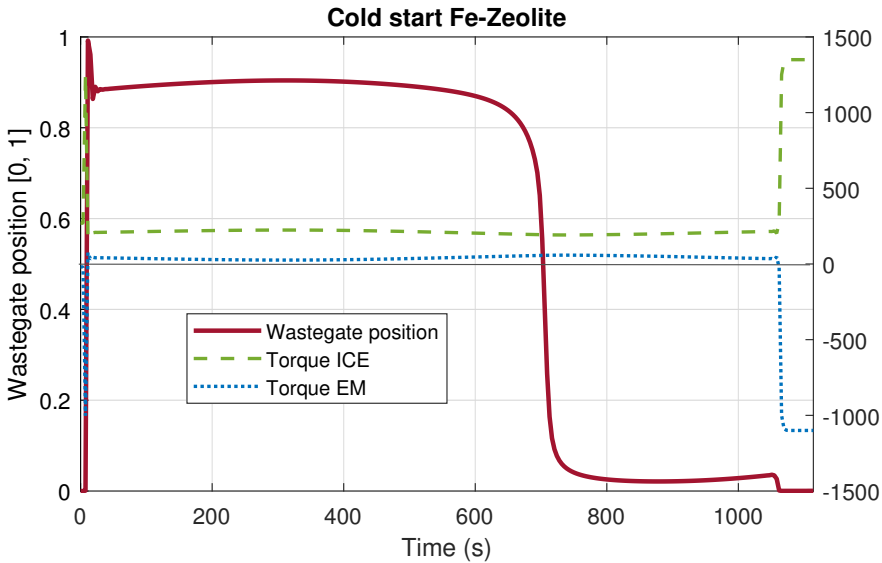


Figure 4.18: Wastegate position and torque-split for the case of a hybrid configuration with Fe-Zeolite catalyst optimized for minimum NO_x emission.

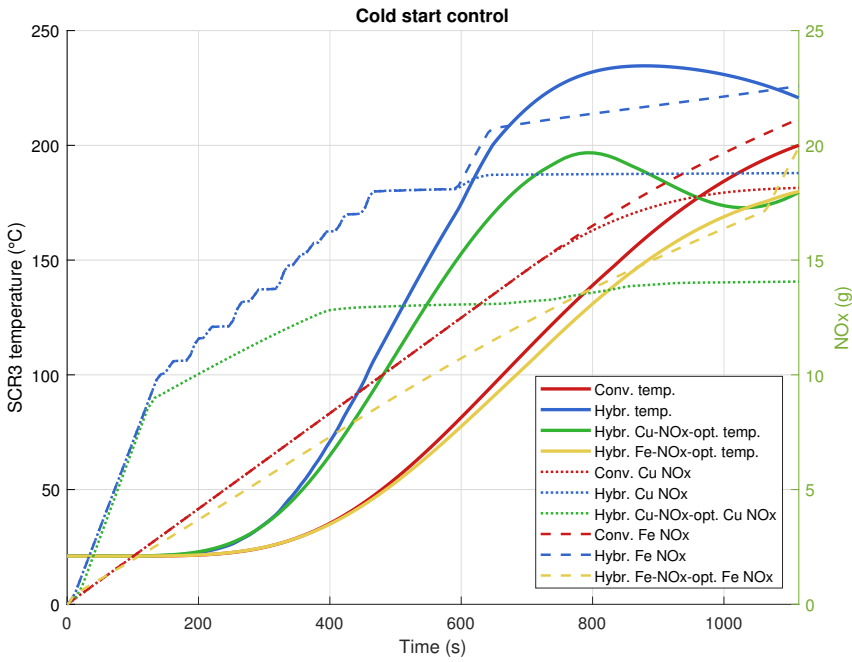


Figure 4.20: Steady state conditions with 250 Nm output torque at 550 rpm. Four cases are compared for temperature in the mid-segment of the SCR, and NO_x emissions for both Cu-Zeolite and Fe-Zeolite catalyst.

Table 4.3: Cold start experiment during steady-state operation at 550 rpm and 250 Nm for several different powertrain setups for comparison.

Experiment	Wastegate	Throttle	Light-off time (s)	Fuel consumed (g)	Cu NO_x emissions (g)	Fe NO_x emissions (g)	Consumed energy (MJ)
Hybrid	×		648	1187	18.79	22.58	50.91
Conventional	×		1114	1034	18.15	21.15	44.36
Hybrid Cu-Z NOx-opt.	×		-	1209	14.07	20.23	51.87
Hybrid Fe-Z NOx-opt.	×		-	1075	16.60	19.91	46.10

4.3 Steady state NO_x versus light-off time tradeoff

The light-off of the catalyst can be expedited by burning additional fuel. By lighting off sooner, more time is spent with the catalyst active. However, whether this strategy is beneficial depends entirely on whether the amount of NO_x removed during this additional activity is greater than the NO_x emitted by the additional fuel spent trying to heat the catalyst. The trade-off between NO_x emissions and light-off time is analyzed in a steady-state operating point of 550 rpm and 250 Nm with a Cu-Zeolite catalyst. The optimization ends when the mid-segment of the SCR catalyst reaches 200 °C.

$$\min_u \quad (1 - \alpha) \cdot t_{end} + \alpha \int_0^{t_{end}} NO_x \, dt$$

$$\begin{aligned} s.t. \quad & 0.25 \leq SOC(t) \leq 0.5 \\ & SOC(t_{end}) \geq 0.375 \\ & SOC(t_0) = 0.375 \\ & M_{ice}(t) + M_{em}(t) = 250 \text{ Nm} \\ & N(t) = 550 \text{ rpm} \\ & T_{SCR3}(t_{end}) = 200 \text{ °C} \end{aligned}$$

The optimization is repeated for different values of the weight factor (α) in order to acquire a set of points. Figure 4.21 visualizes the trade-off curve as well as the corresponding fuel consumption for each point. The curve shows that reducing the light-off time at the expense of fuel is detrimental to NO_x reduction. In fact, the quicker the light-off, the higher the net NO_x emission.

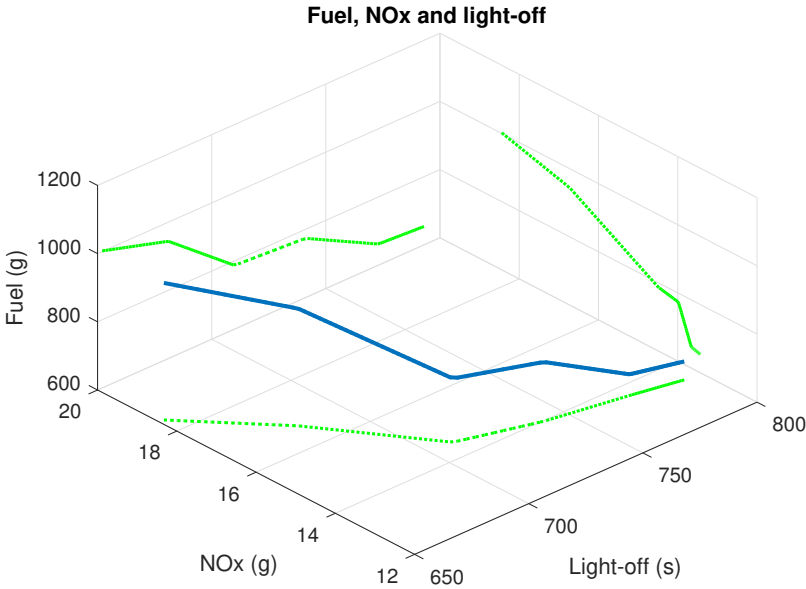


Figure 4.21: Trade-off curve for NO_x and fuel with varying values of α . $\alpha = 0$ on the left-hand side of the blue line, and $\alpha = 1$ on the right-hand side. The green lines are projections of the blue line on the respective plane.

4.4 Steady state fuel versus NO_x trade-off

While it is obvious that burning more fuel increases NO_x emissions, it also increases the temperature, leading to faster catalyst activation which in turn reduces NO_x . This paradoxical relationship raises the question of how much fuel leads to how much NO_x . The phenomenon is analyzed in 1800 second runs of a low steady-state working point of 550 rpm and 250 Nm. By running several optimizations of the same case, but with differing weight in the objective function, a Pareto front can be used to visualize the trade-off between the two variables, as seen in Figure 4.22. The resulting NO_x and fuel values are listed in Table 4.4.

$$\min_u \int_0^{1800} \alpha \cdot W_f + (1 - \alpha) \cdot \text{NO}_x \, dt$$

$$\begin{aligned} \text{s.t.} \quad & 0.25 \leq \text{SOC}(t) \leq 0.5 \\ & \text{SOC}(t_{\text{end}}) \geq 0.375 \\ & \text{SOC}(t_0) = 0.375 \\ & M_{\text{ice}}(t) + M_{\text{em}}(t) = 250 \text{ Nm} \\ & N(t) = 550 \text{ rpm} \end{aligned}$$

Table 4.4: NO_x emission and fuel consumption from 1800 seconds of steadystate operation at 550 rpm and 250 Nm.

α	0	0.1	0.2	0.3	0.4	0.5	0.6	0.7	0.8	0.9	1
NO _x (g)	14.7	17.3	17.36	17.36	17.38	17.43	17.46	17.57	17.70	18.25	20.49
Fuel (kg)	1.89	1.71	1.70	1.70	1.7	1.69	1.69	1.69	1.69	1.68	1.67

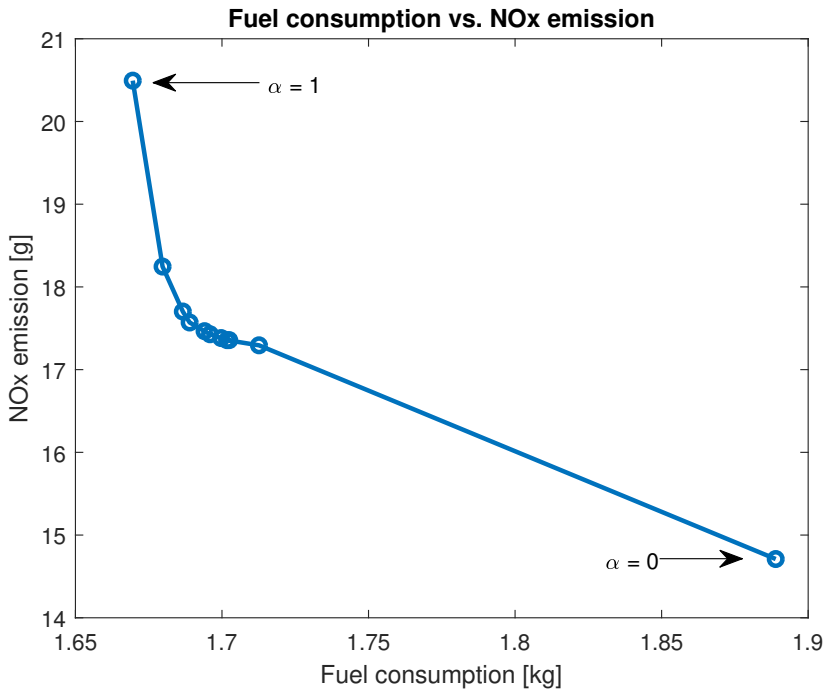


Figure 4.22: Tradeoff curve for NO_x and fuel consumption. The circles represent measurements with falling α .

Optimizing only one of the two variables leads to extreme results. Minimizing fuel consumption leads to large NO_x emissions, and minimizing NO_x requires a large amount of fuel. When combining both variables in the objective function, the results for the different weights are more grouped together. Simply including NO_x with a weight of 0.1 yields a significant decrease in NO_x emission without much additional fuel compared to the fuel optimal case. Further increasing the weight of NO_x in the objective function reveals diminishing returns, with the next large emission reduction occurring only when the weight is 1, and at a significant cost in fuel.

The NO_x optimal solution requires constant action by the powertrain while the fuel optimal strategy is largely passive, as can be seen by the torque for the two extreme cases in Figure 4.23. The corresponding energy usage of these strategies

is displayed in Figure 4.24, and is significantly higher for the NO_x optimal case.

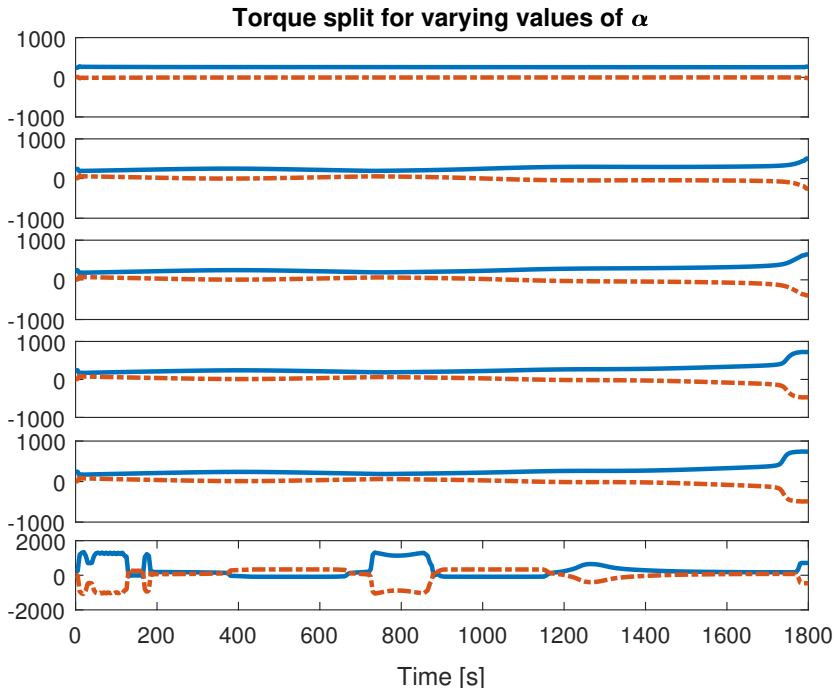


Figure 4.23: ICE and EM torque for α from 1 to 0 in steps of 0.2. The solid blue line represents the ICE and the dash-dotted orange line corresponds to the EM.

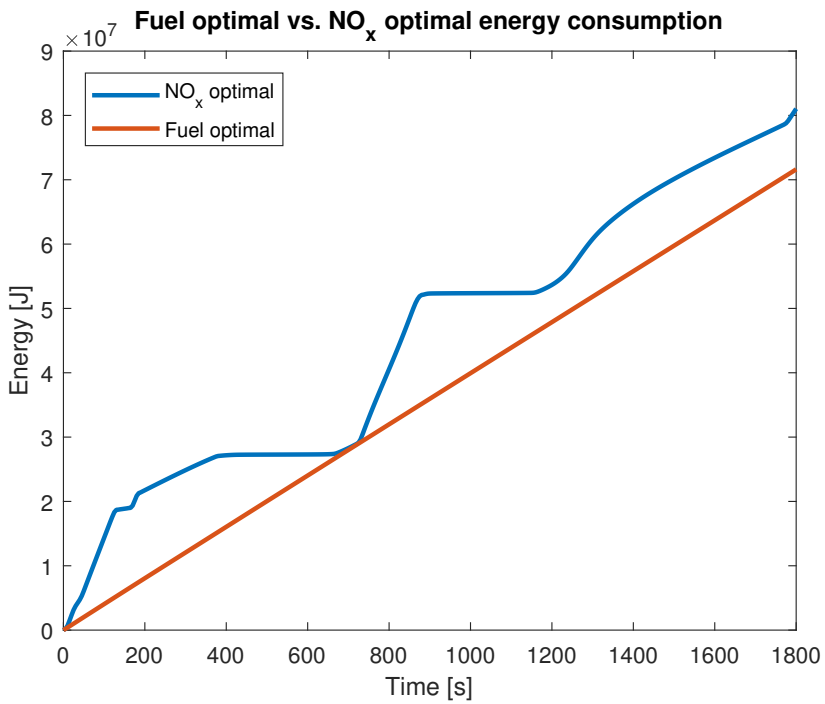


Figure 4.24: Energy usage of fuel optimal and NO_x optimal strategies.

5

Discussion

This thesis proves that numerical optimal control can be a viable tool for analyzing large models. The hybrid configuration with aftertreatment system contains a total of 23 states, and was successfully used in fuel consumption optimization of the WHTC. As a comparison, this number of states is far out of reach for dynamic programming, due to the aforementioned “*curse of dimensionality*”.

The method still has significant limitations. Most notably, some choices of objective are not solvable. For example, when optimizing for minimum tailpipe NO_x emission for the WHTC, no solution is found. A NO_x optimal solution is indeed found when the scenario is limited to up to the first 150 seconds of the WHTC cycle, but this timespan is too short to gather any useful information due to the slow temperature dynamics of the aftertreatment system.

Attempting to remedy these issues reveals that increasing the tolerances sometimes yields a solution that is considered optimal by the solver where no solution was previously found. These solutions are often physically nonsensical, possibly due to the low tolerances as the solver may find a local optimum satisfying the tolerances even though there are other local or global optimal solutions nearby. It may also be that the solver has exploited some weakness in the model. As an example of this, using NO_x maps with PPM as their unit and multiplying with mass flow in order to integrate the product for total NO_x over the cycle, results in the optimizer trying to limit the massflow since the NO_x value is fixed by the working point from the cycle. Furthermore, increasing and decreasing the number of collocation points and intervals yields no conclusive results.

Other approaches were tried for the initial guess for the solver, see Appendix B. However, after many optimizations for benchmarking purposes it was found that a better initial guess does not always improve the stability and performance of

the solver which was initially assumed. Therefore, the same initial guess that was used for the conventional powertrain was used for the hybrid configuration when optimizing for the presented results.

This leaves the model complexity as a likely cause for the optimization difficulties. Since fuel consumption can be controlled directly by the fuel injection control signal, minimizing it is relatively straightforward. NO_x on the other hand depends largely on temperature, the dynamics of which are very slow and dependent on a large number of variables such as fuel injection, wastegate position and torque-split, making it more difficult to control. It is therefore reasonable to assume that a less complex model would be better supported by the methods utilized in this thesis.

However, since successful optimizations of NO_x during steady-state conditions were performed, the model is not the only factor influencing whether the problem is solvable or not. Rather, the combination of models and driving mission seems to determine whether the problem can be solved.

In Figure 4.7 oscillations can be seen for the wastegate position. When lowering the tolerances of the solver, some oscillation was eliminated. However, very stringent tolerances increase the optimization time drastically. Despite these oscillations, the general behavior is expected to be maintained even though the tolerances give room for more slack.

In section 4.1 it becomes clear that for the WHTC cycle, high temperatures are as problematic as low ones when using the Cu-Zeolite catalyst and optimizing for fuel efficiency. While the Cu-Zeolite catalyst lights off slightly faster than the Fe-Zeolite catalyst, it quickly loses activity due to the upper limit of its temperature range being exceeded. Carefully controlling the maximum temperature could therefore lead to more consistent deNO_x performance than trying to light-off quickly. The Fe-Zeolite catalyst, on the other hand, maintains its high activity at higher temperatures. This means that a quicker light-off is the only way of increasing its performance if the driving cycle is demanding enough to maintain the temperatures required for good Fe-Zeolite deNO_x performance. It is clear that for the fuel optimal WHTC, the Fe-Zeolite catalyst is better suited regardless of whether a hybrid or conventional powertrain is used.

The steady state experiments in section 4.2, where NO_x was successfully optimized, shows that a pulsating temperature that stays within the active range of the Cu-Zeolite catalyst leads to less NO_x than the case of a minimized light-off time followed by minimized fuel consumption to which it was compared. This despite the fact that the NO_x optimal case is the last one to reach the light-off temperature of 200 °C. It can therefore be concluded that the matter of minimizing NO_x is not as simple as just activating the catalyst as quickly as possible, but that both timing and quantity of injected fuel is of essence. The deNO_x performance is similar for all three cases once the catalyst is active.

6

Conclusions

A reasonable assumption is that decreasing the light-off time for the SCR catalyst during cold starts leads to decreased NO_x emission. The results of this work implies that this is not necessarily the case, but that there is a trade-off between light-off time and NO_x produced during the heating phase. If the engine is forced to light-off at an accelerated pace by burning more fuel, it might as well increase the overall NO_x emission, contradicting the very purpose of taking heating measures. Careful consideration should be taken to this trade-off when designing an engine control system.

One reoccurring behavior observed during cold starts is that the engine goes through a brief heating phase before closing the wastegate, thus pushing the heat gases through the exhaust system as the turbocharger is increasing the massflow. The best controls for minimizing NO_x takes advantage of the slow thermal dynamics of the exhaust system and waits for the heat produced in the heating phase to reach the SCR before loading the engine once more. The best engine control system should mimic this behavior for reducing cold start NO_x emission.

It is also shown that the optimal controls for minimizing NO_x emissions does lead to an increased fuel consumption compared to the case of optimized controls for fuel efficiency. However, the percentage amount of fuel savings are far less than the percentage of NO_x emission reduction available when comparing the two ways of controlling the powertrain.

The hypothesis that the exhaust system temperatures during WHTC would be lower for the hybrid configuration than for the conventional configuration is confirmed. However, the deNO_x performance is better for the hybrid configuration, both for Cu-Zeolite and Fe-Zeolite, even though the temperatures are lower. The

temperatures achieved during WHTC is higher than beforehand expected and the reduction in temperature that the hybrid configuration exhibits compared to the conventional powertrain improves the deNO_x performance.

6.1 Future work

- Including the throttle in the optimizations may reveal interesting behavior.
- A complete vehicle model would allow for a more adequate description of regenerative braking using kinetic energy.
- Implementing sub-optimal injection timing, which deliberately lowers the efficiency of the engine and thus increases temperature, would provide an interesting additional case for investigation.
- A model of an actual HEV truck battery would likely be better dimensioned than the current model, which is dimensioned with respect to the maximum power of the electric motor and has a relatively low capacity.
- Parameterizing the aftertreatment system to represent a production model would provide more accurate and comparable results. Expanding the models to account for gas mixture and space velocity could further improve their veracity.
- Running other driving cycles than the WHTC could possibly enable some of the combinations of cycle and objective function that have thus far failed. For instance, optimizing NO_x during WHTC is not possible, but optimizing NO_x in a steady-state working point is. Trying smoother, simpler cycles may help in finding the limit where the complexity presents too much of a challenge for the optimizer.
- Replacing lookup tables with continuous functions would increase computational speed. Additionally, it would enable use of the direct multiple shooting algorithm, allowing for comparison between the two optimization methods (the other being direct collocation), and at best solve problems that DC can not.
- Defining what the optimization environment can and can not solve would reduce wasted time during usage drastically.

Appendix

A

WHTC denormalization

WHTC is given as percentage values of engine speed and output torque. Using the engine map for the engine to be tested, the cycle is denormalized according to Section A.1 and A.2 using the same procedure as described by the United Nations test procedure [30].

A.1 Engine speed profile

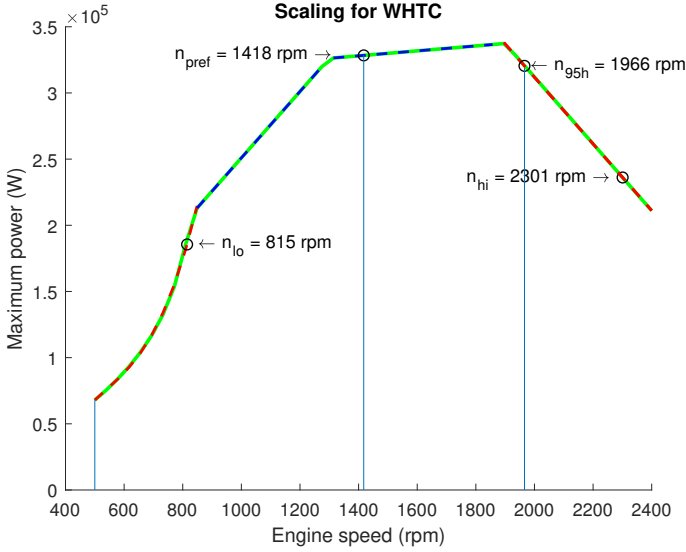
The denormalization for the WHTC engine speed is described according to equation (A.1).

$$speed = 2.0327n_{norm} \cdot (0.45n_{lo} + 0.45n_{pref} + 0.1n_{hi} - n_{idle}) + n_{idle} \quad (A.1)$$

Where n_{idle} is the idle speed and n_{norm} is the vector of speed percentage values for the WHTC. n_{lo} is the lowest engine speed where 55% of the maximum power is produced. n_{hi} is the highest engine speed where 70% of the maximum power is produced. n_{pref} is the engine speed where the integral from n_{idle} to n_{pref} equals 51% of the integral from n_{idle} to n_{95} , whereas n_{95} is the highest engine speed where 95% of the maximum power is produced. The values for each of these engine speeds are presented in table A.1. Figure A.1 shows the maximum power as a function of engine speed where all engine speeds are presented that are used in the denormalization of the engine speed for WHTC.

Table A.1: Engine speeds used for denormalization of WHTC engine speed.

n_{idle}	=	500	rpm
n_{lo}	=	815	rpm
n_{pref}	=	1418	rpm
n_{95}	=	1966	rpm
n_{hi}	=	2301	rpm

**Figure A.1:** Finding values of engine speed corresponding to the values required to denormalize the WHTC speed profile.

A.2 Torque profile

The torque profile of WHTC ranges from -10% to 100% torque. The negative values represent as much engine braking that is available at the specific engine speed. As the WHTC test procedure is designed for conventional combustion engines, no consideration is taken for regenerative braking using the electric motor as a generator during negative torque sections. However, as the considered powertrain is an electric hybrid, regenerative braking is added. 100% torque is the maximum torque the diesel engine can deliver which is 2400 Nm. The denormalization procedure for all positive torque values can be described by equation A.2 [30].

$$torque = M_{norm} \cdot M_{max/n}/100 \quad (A.2)$$

M_{norm} is the vector of torque percentage values for the WHTC and $M_{max/n}$ is the maximum torque available at the current engine speed. During negative torque periods, the electric machine is assumed to utilize 1000 Nm of torque when the engine speed is below about 1600 rpm. Above 1600 rpm the maximum power that can be generated from the electric motor will be saturated and the regenerative torque will thus drop gradually as the engine speed increases, see Figure (3.7).

B

Solver initial guess - Alternative approaches

To improve the solveability of the optimizer, several attempts were conducted to improve the initial guess for the solver. These include a constant torque-split with a proportional controller on state of charge deviation from the initial value and ECMS.

B.1 Constant torque-split with feedback

During torque delivery, $(1 - \gamma) \cdot M_{demand}$ is to be delivered by the conventional engine and the remaining $\gamma \cdot M_{demand}$ from the electric motor. During engine braking the electric motor is to handle all of the required braking torque. γ is a function of SOC and α , a chosen percentage value according to Equation (B.1).

$$\gamma = \alpha - \alpha \frac{SOC_{init} - SOC}{SOC_{max,diff}} \quad (B.1)$$

α is chosen such that the truck is charge-sustaining. For a simulation of the whole 1800 second WHTC, an α value of 28% is appropriate. SOC_{init} is the initial state of charge which is 0.375. $SOC_{max,diff}$ is $0.5 - 0.375 = 0.125$ and it is the maximum allowed difference from SOC_{init} to current state of charge, SOC . This algorithm will adjust the torque-split so that the state of charge strives to remain within its limits as can be seen in Equation (B.2), while using the electric motor somewhat alike the ECMS way. This algorithm does however suffer from

not knowing if any constraints are violated during the simulation.

$$\begin{aligned}
 SOC = 0.5 & : \gamma = \alpha + \frac{0.125 \cdot \alpha}{0.125} = 2\alpha \\
 SOC = 0.375 & : \gamma = \alpha \\
 SOC = 0.25 & : \gamma = \alpha - \frac{0.125 \cdot \alpha}{0.125} = 0
 \end{aligned} \tag{B.2}$$

To be able to determine if the initial guess violated any constraints, the model was run at every time-step with inputs from the initial guess. In each time-step the constraints were checked for violation. In the occurrence of a violation, the guessed control vector for the initial guess was adjusted and the initial guess was checked again.

B.2 Equivalent Consumption Minimization Strategy

Attempts were made to use ECMS for the initial guess for the hybrid configuration, see chapter 1, section 1.2. The model was simulated using the same methods as for the conventional engine. However, in each time-step in the simulation the hamiltonian (H) was minimized. The result is an optimal torque-split considering current state of charge, torque demand, chosen equivalence factor (λ) among other variables, Equation (B.3). The dividing of torque between the electric motor and the diesel engine was performed without consideration to model constraints, which were often violated as a result. Therefore, the solution received was not eligible as an initial guess for the optimization. Despite this, ECMS could be used for benchmark purposes.

$$\begin{aligned}
 u^*(t) &= \arg \min_u H(t, u, \lambda) \\
 H(t, u, \lambda) &= P_f(t, u) + \lambda P_{ech}(t, u) \\
 \text{s.t. } M_{ice}(t) + M_{em}(t) &= M_{dem}(t)
 \end{aligned} \tag{B.3}$$

It is however necessary to optimize the whole cycle minimizing the integral of the hamiltonian over the entire cycle, as per Equation (B.4). In this way, the torque-split in each time-step strives to minimize the hamiltonian whilst ensuring that all constraints are met throughout the cycle.

$$\begin{aligned}
u^* &= \arg \min_u \int_0^{t_{end}} H(t, u, \lambda) dt \\
H(t, u, \lambda) &= P_f(t, u) + \lambda P_{ech}(t, u) \\
\text{s.t. } &M_{ice}(t) + M_{em}(t) = M_{dem}(t)
\end{aligned} \tag{B.4}$$

Furthermore, finding the appropriate equivalence factor for sustaining the battery charge requires many optimizations to be run for tuning in the equivalence factor. By extending the control vector, the equivalence factor becomes an optimization variable. Setting the derivative of the equivalence factor to *zero* and optimizing the equivalence factor to achieve charge-sustainability whilst minimizing the hamiltonian, the optimizer constantly increases the equivalence factor to the highest allowed value and forcing the model to be charge-sustaining through altering the torque-split. While this behavior minimized the objective function, it is not considered equal to *ECMS*.

Adjusting the equivalence factor through a proportional feedback by 1.5 times the difference between the final state of charge and the initial state of charge for each consecutive optimization is a functional approach. However, this method still suffers from very long computational times as many optimizations must be conducted to adjust the equivalence factor so that the state of charge ends up within acceptable tolerances from the initial state of charge. Another approach could be to utilize parallel computing through use of the *Bisection method* to find the appropriate equivalence factor [5]. However, as the solver does not consistently converge to a plausible solution, the equivalence factor may not converge to an appropriate value.

Bibliography

- [1] United States Environmental Protection Agency and National Highway Traffic Safety Administration. EPA and NHTSA adopt standards to reduce greenhouse gas emissions and improve fuel efficiency of medium- and heavy-duty vehicles for model year 2018 and beyond. *Office of Transportation and Air Quality*, EPA-420-F-16-044, 2016. Cited on page 15.
- [2] Joakim Andersson. Lifetime estimation of lithium-ion batteries for stationary energy storage systems. *Vattenfall R&D*, KTH, 2017. Cited on page 25.
- [3] European Automobile Manufacturers Association. Diesel exhaust fluid - AdBlue. <http://www.acea.be/industry-topics/tag/category/diesel-exhaust-fluid-adblue>, 2018. Accessed: 2018-02-06. Cited on page 11.
- [4] Richard Bellman. The theory of dynamic programming. *Bull. Amer. Math. Soc.*, 60:1–19, 1954. Cited on page 2.
- [5] Richard L. Burden and J. Douglas Faires. *Numerical Analysis*. Brooks/Cole, Cengage Learning, ninth edition, 2010. ISBN -13: 978-0-538-73351-9. Cited on page 75.
- [6] J. Girard, G. Cavataio and C. K. Lambert. The influence of ammonia slip catalysts on Ammonia, N_2O and NO_x emissions for diesel engines. *SAE International: Diesel Exhaust Emissions Control*, ISSN 0148-7191(SP-2080), 2007. Cited on page 12.
- [7] N. Kim, S. Cha, and H. Peng. Optimal control of hybrid electric vehicles based on pontryagin's minimum principle. *IEEE Transactions on Control Systems Technology*, 19(5):1279–1287, 2011. Cited on pages 1 and 2.
- [8] J.H. Baik, S.D. Yim, I Nam, Y.S. Mok, J. Lee, B.K. Cho, and S.H. Oh. Control of NO_x emissions from diesel engine by selective catalytic reduction (SCR) with urea. *Topics in Catalysis*, 30/31(1–4):37–41, 2004. Cited on page 10.
- [9] S.D. Yim, S.J. Kim, J.H. Baik, I. Nam, Y.S. Mok, J. Lee, B.K. Cho, and S.H. Oh. Decomposition of urea into NH_3 for the SCR process. *Industrial & Engineering Chemistry Research*, 43:4856–4863, 2004. Cited on page 12.

- [10] I. Chorkendorff and J.W. Niemantsverdriet. *Concepts of Modern Catalysis and Kinetics*. WILEY-VCH Verlag GmbH & Co. KGaA, Weinheim, second edition, 2007. Cited on page 5.
- [11] Chevron Corporation. Diesel fuels technical review. <https://www.chevron.com/-/media/chevron/operations/documents/diesel-fuel-tech-review.pdf>, 2007. Cited on page 7.
- [12] dieselnet.com. EU: Heavy-duty truck and bus engines. <https://www.dieselnet.com/standards/eu/hd.php#stds>, 2016. Accessed: 2018-01-17. Cited on page 14.
- [13] Z. Yuan, L. Teng, S. Fengchun, and H. Peng. Comparative study of dynamic programming and pontryagin's minimum principle on energy management for a parallel hybrid electric vehicle. *Energies*, 6(4):2306–2317, 2013. Cited on pages 2 and 3.
- [14] Agency for Toxic Substances and Disease Registry. Public health statement - Ammonia. *Division of Toxicology*, CAS#:(7664-41-7), 2004. Cited on page 12.
- [15] James A. Raub , Monique Mathieu-Nolf, Neil B. Hampson and Stephen R. Thom. Carbon monoxide poisoning — a public health perspective. *Toxicology*, 145(1):1–14, 2000. Cited on page 7.
- [16] International Plant Nutrition Institute. Ammonia. *Nutrient Source Specifics*, NSS-10. Cited on page 10.
- [17] Masaoki Iwasaki and Hirofumi Shinjoh. A comparative study of “standard”, “fast” and “NO₂” SCR reactions over Fe/zeolite catalyst. *Applied Catalysis A: General*, 390(1–2):71–77, 2010. Cited on pages 7, 10, and 11.
- [18] K. Daneshvar, R. K. Dadi, D. Luss, V. Balakotaiah, S. B. Kang, C. M. Kalamaras and W. S. Epling. Experimental and modeling study of CO and hydrocarbons light-off on various Pt-Pd/ γ -Al₂O₃ diesel oxidation catalysts. *Chemical Engineering Journal*, 323:347–360, 2017. Cited on page 9.
- [19] Peter M. Kleemann. Beschichtung von cordierit-wabenkörpern für die selektive katalytische reduktion von stickoxiden. *Diss. Eth.*, 13401, 1999. Cited on page 13.
- [20] M. Kleemann, M. Elsener, M. Koebel and A. Wokaun. Hydrolysis of Isocyanic Acid on SCR Catalysts. *Industrial & Engineering Chemistry Research*, 39:4120–4126, 2000. Cited on page 12.
- [21] M. Lemmetty, H. Vehkamäki, A. Virtanen, M. Kulmala and J. Keskinen. Homogeneous Ternary H₂SO₄ – NH₃ – H₂O Nucleation and Diesel Exhaust: a Classical Approach. *Lemmetty et al. Aerosol and Air Quality Research*, 7(4): 489–499, 2007. Cited on page 12.

- [22] P. Korhonen, M. Kulmala, A. Laaksonen and Y. Viisanen. Ternary nucleation of H_2SO_4 , NH_3 and H_2O in the atmosphere. *Journal of Geophysical Research*, 104(D21):26,349–26,353, 1999. Cited on page 12.
- [23] J. Jeon, J.-T. Lee and S. Park. Nitrogen compounds (NO, NO₂, N₂O, and NH₃) in NO_x emissions from commercial EURO VI type heavy-duty diesel engines with a urea-selective catalytic reduction system. *Energy Fuels*, 30(8):6828–6834, 2016. Cited on page 6.
- [24] Kristoffer Ekberg, Viktor Leek and Lars Eriksson. Optimal control of wastegate throttle and fuel injection for a heavy-duty turbocharged diesel engine during tip-in. *SAE Technical Papers*, 2017-01-0611:317–325, 2017. Cited on page 25.
- [25] Viktor Leek. An optimal control toolbox for MATLAB based on CasADi. ISRN: LiTH-ISY-EX-16/4986-SE, 2016. Cited on page 17.
- [26] Bin Guan, Reggie Zhan, He Lin and Zhen Huang. Review of state of the art technologies of selective catalytic reduction of NO_x from diesel engine exhaust. *Applied Thermal Engineering*, 66(1-2):395–414, 2014. Cited on pages 30 and 31.
- [27] R. Wang, S.-M. Lukic. Dynamic programming technique in hybrid electric vehicle optimization. *IEEE International Electric Vehicle Conference*, pages 1–8, 2012. Cited on page 2.
- [28] Yao Ma and Junmin Wang. Integrated Power Management and Aftertreatment System Control for Hybrid Electric Vehicles with Road Grade Preview. *IEEE Transactions on Vehicular Technology*, 66(12):10,935–10,945, 2017. Cited on page 3.
- [29] J.R. Belt, C.D. Ho, C.G. Motloch, T.J. Miller and T.Q. Duong. A capacity and power fade study of Li-ion cells during life cycle testing. *Journal of Power Sources*, 123:241–246, 2003. Cited on page 25.
- [30] United Nations. Test procedure for compression-ignition (C.I.) engines and positive ignition (P.I.) engines fuelled with natural gas (NG) or liquefied petroleum gas (LPG) with regard to the emission of pollutants. *Established in the Global Registry on 15 November 2006*, ECE/TRANS/180/Add.4, 2006. Cited on pages 15, 69, and 70.
- [31] C.-L. Myung, A. Ko, J. Kim, K. Choi, S. Kwon, S. Park. Specific engine performance and gaseous emissions characteristics of european test cycle and worldwide harmonized driving cycle for a heavy-duty diesel engine. *Journal of Mechanical Science and Technology*, 27(12):3893–3902, 2013. Cited on page 14.
- [32] L. Serrao, A. Sciarretta, O. Grondin, A. Chasse, Y. Creff, D. Di Domenico, P. Pognant-Gros, C. Querel, and L. Thibault. Open issues in supervisory control of hybrid electric vehicles: A unified approach using optimal control

- methods. *Oil & Gas Science and Technology*, 68(1):23–33, 2011. Cited on page 3.
- [33] April Russel and William S. Epling. Diesel oxidation catalysts. *Catalysis Reviews*, 53(4):337–423, 2011. Cited on page 9.
- [34] J. Kessels, F. Willems, W. Schoot and P. van den Bosch. Integrated energy & emission management for hybrid electric truck with SCR aftertreatment. *Vehicle Power and Propulsion Conference (VPPC), 2010 IEEE*, 2010. Cited on page 3.
- [35] J. Girard, G. Cavataio, R. Snow and C. Lambert. Combined Fe-Cu SCR systems with optimized ammonia to NOx ratio for diesel NOx control. *SAE Int. J. Fuels Lubr.*, 1(1):603–610, 2008. Cited on page 6.
- [36] M. Koebel, E.O. Strutz. Thermal and Hydrolytic Decomposition of Urea for Automotive Selective Catalytic Reduction Systems: Thermochemical and Practical Aspects. *Industrial & Engineering Chemistry Research*, 42:2093–2100, 2003. Cited on pages 11 and 12.
- [37] S. Solomon, D. Qin, M. Manning, Z. Chen, M. Marquis, K.B. Averyt, M. Tignor and H.L. Miller. Contribution of working group I to the fourth assessment report of the intergovernmental panel on climate change. *Climate Change 2007 - The Physical Science Basis*, ISBN 978-0-521-70596-7 (ISBN 978 0521 88009-1):212–213, 2007. Cited on page 13.
- [38] E. Hünnekes, P. van der Heijden and J. Patchett. Ammonia Oxidation Catalysts for Mobile SCR Systems. *SAE Technical Paper Series*, ISBN 0-7680-1717-3, 2006. Cited on pages 13 and 14.
- [39] Andreas Wächter and Carl Laird. IPOPT. <https://projects.coin-or.org/Ipopt>, Accessed: 2018-03-19. Cited on page 17.
- [40] Joel Andersson, Johan Åkesson, Joris Gillis, Moritz Diehl. CasADi. <https://github.com/casadi/casadi/wiki>, Accessed: 2018-02-22. Cited on page 17.
- [41] P.-E. Schwarze, J. Øvrevik, M. Låg, M. Refsnes, P. Nafstad, R.-B. Hetland and E. Dybing. Particulate matter properties and health effects: consistency of epidemiological and toxicological studies. *Human & Experimental Toxicology*, 205(1):559–579, 2006. Cited on page 7.

Index

- NO₂/NO_x ratio, 10
- ADBlue, 3
- AdBlue, 10
- Aerosols, 12
- Aftertreatment system, 28
- Ammonia, 10
- Ammonia slip, 12
- Ammonia slip catalyst, 12
- Arrhenius equation, 5
- ASC, 12
- ASC
 - abbreviation, ix
- ASC reactions, 14
- Battery, 24
- Battery capacity, 25
- Battery voltage, 24
- BMS, 24
- BMS
 - abbreviation, ix
- Carbon monoxides, 7
- CasADi, 17
- Catalysis, 5
- Catalyst, 30
- Cold start optimal control, 39
- Conclusions, 65
- Cu-Zeolite, 6, 30
- DEF, 10
- DEF
 - abbreviation, ix
- Denormalization of WHTC, 21
- deNO_x, 29
- Development procedure, 17
- Diesel engine, 25
- Diesel oxidation catalyst, 9
- Diesel particulate filter, 9
- Direct collocation, 4
- Direct methods, 3
- Direct multiple shooting, 3
- Discussion, 63
- DOC, 9
- DOC
 - abbreviation, ix
- DP
 - abbreviation, ix
- DPF, 9
- DPF
 - abbreviation, ix
- Dynamic programming, 2
- EATS, 28
- EATS
 - abbreviation, ix
- ECMS, 1, 2
- ECMS
 - abbreviation, ix
- ECMS as initial guess, 74
- Electric motor, 22
- EM, 1
- EM
 - abbreviation, ix
- Emission standards, 14
- Emissions and aftertreatment, 7
- EPA, 15
- EPA

- abbreviation, ix
- EURO VI, 14
- Fe-Zeolite, 6, 30
- FTP
 - abbreviation, ix
- Future work, 66
- Hamiltonian, 3
- HD
 - abbreviation, ix
- HEV, 1
- HEV
 - abbreviation, ix
- High load operating point, 39
- HNCO, 11
- Hydrocarbons, 7
- ICE, 1
- ICE
 - abbreviation, ix
- Interpolant ripples, 19
- IPOPT, 17
- Isocyanid acid, 11
- LiFePO₄, 24
- Light-off, 30
- LiU-Diesel 2, 25
- Lookup tables, 18
- Low load operating point, 48
- Model controls, 27
- Model description, 21
- Model states, 25
- NHTSA, 15
- NHTSA
 - abbreviation, ix
- Nitric oxide, 7
- Nitrogen dioxide, 7
- NLP
 - abbreviation, ix
- NO_x, 27
- NO_x
 - abbreviation, ix
- Objective, 1
- OCP
 - abbreviation, ix
- Open circuit voltage, 25
- Optimization environment, 17
- Optimization limitations, 32
- Particulate matter, 7
- Piecewise linear, 21
- PM
 - abbreviation, ix
- PM regeneration, 9
- PMP
 - abbreviation, ix
- Pontryagin's minimum principle, 2
- Power distribution, 2
- Regenerative braking, 71
- Related research, 2
- Results, 33
- SCR, 10
- SCR
 - abbreviation, ix
- SCR reactions, 10
- Selective catalytic reduction, 10
- SOC, 25
- SOC
 - abbreviation, ix
- Solver initial guess, 21
- Space velocity, 10
- Steady state fuel vs. NO_x, 58
- Steady state NO_x vs. LO-time, 57
- Temperature comparison, 33
- Theory and background, 5
- Urea, 10
- Urea injection and decomposition, 10
- WHSC
 - abbreviation, ix
- WHTC, 14
- WHTC
 - abbreviation, ix
- WHTC denormalization, 69
- WHTS, 14